

Quantifying the Effects of Contact Tracing, Testing, and Containment Measures in the Presence of Infection Hotspots

Lars Lorch*, Heiner Kremer[†], William Trouleau[‡], Stratis Tsirtsis[§], Aron Szanto[¶],
Bernhard Schölkopf^{†,*}, Manuel Gomez-Rodriguez[§]

*ETH Zürich, lloch@student.ethz.ch

[†]Max Planck Institute for Intelligent Systems, {heiner.kremer,bs}@tuebingen.mpg.de

[‡]École Polytechnique Fédérale de Lausanne, william.trouleau@epfl.ch

[§]Max Planck Institute for Software Systems, {stsirtsis,manuelgr}@mpi-sws.org

[¶]Zerobase Foundation, aron@zerobase.io

November 27, 2021

Abstract

Multiple lines of evidence at the individual and population level strongly suggest that infection hotspots, or *superspreading events*, where a single individual infects many others, play a key role in the transmission dynamics of COVID-19. However, most of the existing epidemiological models either assume or result in a Poisson distribution of the number of infections caused by a single infectious individual, often called secondary infections. As a result, these models overlook the observed overdispersion in the number of secondary infections and are unable to accurately characterize infection hotspots. In this work, we aim to fill this gap by introducing a temporal point process framework that explicitly represents sites where infection hotspots may occur. Under our model, overdispersion on the number of secondary infections emerges naturally. Moreover, using an efficient sampling algorithm, we demonstrate how to apply Bayesian optimization with longitudinal case data to estimate the transmission rate of infectious individuals at sites they visit and in their households, as well as the mobility reduction due to social distancing. Simulations using fine-grained demographic data and site locations from several cities and regions demonstrate that our framework¹ faithfully characterizes the observed longitudinal trend of COVID-19 cases. In addition, the simulations show that our model can be used to estimate the effect of testing, contact tracing, and containment at an unprecedented spatiotemporal resolution, and reveal that these measures do not decrease overdispersion in the number of secondary infections.

1 Introduction

As countries around the world aim to counteract rising numbers of COVID-19 infections [1–3], overwhelmingly growing evidence suggests that few infected people in infection hotspots, or *superspreading events* (SSEs), may be responsible for both explosive early growth of cases and sustained transmission in later stages [4–9]. For example, in Hong Kong, the largest infection hotspots were traced back to four bars, which accounted for 32.5% of all locally acquired infections from January 23 to April 28, 2020 [4]. In South Korea, an infection hotspot linked to a church was responsible for at least 60% of all recorded cases by March 18, 2020, and over 1,000 infections were traced back to a single individual [10]. The first major outbreak in Germany occurred after an infected couple attended a carnival festivity in Heinsberg, with superspreading dynamics later verified from virus genome sequencing [11]. These lines of evidence suggests that, for COVID-19, the number of secondary infections caused by a single individual is *overdispersed*—most individuals infect few and a few infect many [12–14].

¹Our code is publicly available at: <https://github.com/covid19-model/>

Most of the existing epidemiological models, including those developed and used in the context of the COVID-19 pandemic, either assume or result in a Poisson distribution of infections caused by an individual and do not explicitly represent sites of transmission. As Poisson distributions have the same mean and variance, this seemingly justifies containment measures that merely aim to reduce the effective reproduction number, *i.e.*, the *average* number of infections caused by an individual. However, due to the overdispersion observed for COVID-19², these models have been of little use for identifying conditions under which hotspots emerge [8, 12], helping design control measures tailored to prevent SSEs [18], or predicting where infection hotspots are most likely to occur [14].

In this work, we take a first step towards addressing the above limitations and develop a flexible modeling framework that explicitly represents visits to sites where infections occur and hotspots may emerge. In particular, to realistically model the exposure of individuals at sites, our framework introduces

- (i) a “check-in” mobility model that characterizes the frequency and duration of each individual’s visits to specific sites, which can be configured using a variety of publicly available data
- (ii) a new rate of transmission at sites that quantifies the influence of environmental drivers, individual mobility patterns, and containment measures on the risk that each infected individual poses to their community.

By using this new rate of transmission and an explicit representation of sites, our framework can naturally exhibit overdispersion of secondary infections, *i.e.*, without explicitly encoding it, as shown in Figures 3 and 6. Our model uses temporal point processes [19] to represent events when individuals

- ... check in at different sites, where they get in contact with and infect each other, possibly creating infection hotspots (*Mobility*).
- ... become exposed, asymptomatic, presymptomatic, symptomatic, hospitalized, recovered, or die (*Epidemiology*).
- ... are affected by measures such as social distancing and quarantines, or sites implement hygienic and capacity-limiting policies (*Containment measures*).
- ... get tested or receive the outcome of a test (*Testing*).

The efficient sampling algorithm for our model allows us to simulate the spread of COVID-19 in real-world cities and regions with hundreds of thousands of inhabitants under a variety of interventions and what-if scenarios. Building on this procedure, we demonstrate how to apply Bayesian optimization [20–22] with longitudinal COVID-19 case data to estimate the model parameters that control transmissions at sites. Finally, we showcase our method using fine-grained demographic data and site locations from several cities and regions in Germany and Switzerland. Our results demonstrate that our model can faithfully characterize real COVID-19 case trends and be used to estimate the effect of testing, contact tracing, and containment at an unprecedented spatiotemporal resolution. Moreover, they also reveal that these interventional measures do not decrease overdispersion in secondary infections. To facilitate research in this area, we release the implementation of our framework that includes the code required to run simulations in any desired region.

Related work Most of the classical epidemiological literature has focused on developing population models [23, 24], unable to capture heterogeneous transmission dynamics at the individual level. More recently, there has been research on agent-based epidemic modeling [25–29], also in the context of COVID-19 [30–36]. These models predominantly use multi-layer contact networks, discrete time, meta-populations, or Poisson transmission rate assumptions to characterize individual infections, rather than the frequency and duration of each individual’s visits to specific sites, as our model does. Two notable exceptions are by Aleta et al. [37], who use check-in data of real sites, yet only to configure the layers of a multi-layer contact network, and Ferreti et al. [38], who employ a time-varying transmission rate, but ultimately average over individuals who infect few or many others. However, none of the above models, including these two exceptions, are

²Overdispersion has been also observed in MERS and SARS outbreaks [15–17].

able to characterize the overdispersion in secondary infections that has been identified as a root cause of SSEs [4, 6–8]. In contrast, our model presents a paradigm shift in individual-level epidemic modeling, under which overdispersion in the number of secondary infections naturally emerges.

2 A Spatiotemporal Epidemic Model

Given a set of individuals \mathcal{V} , we track the current state of each single individual $i \in \mathcal{V}$ using a collection of state variables, which determine their mobility pattern, epidemiological condition, and testing status. The state transitions are modeled using stochastic differential equations (SDEs) with jumps, which faithfully captures (i) the stochastic nature of infection events and mobility patterns, (ii) events in continuous time, i.e. *not* in aggregate over a time period, and (iii) discrete state transitions—an individual either does *or* does not get infected, visit a site, or is tested positively.

Specifically, the jumps are modeled using counting processes [19], say $N(t)$, which record the number of discrete events in time $\{t_1, t_2, \dots, t_n\}$, $t_i \in \mathbb{R}_+$ before time t . The probability of an event occurring in a small time window $[t, t + dt)$ is given by $P(dN(t) = 1 | \mathcal{H}(t)) = \lambda(t) dt$ with $dN(t) \in \{0, 1\}$, history of events $\mathcal{H}(t)$, and conditional intensity function $\lambda(t)$, which can be interpreted as the instantaneous rate of events per unit of time. To ease the exposition, we describe the different types of state variables separately.

Mobility Let \mathcal{S} be the set of *sites* individuals can visit. For each individual i , let the indicator $P_{i,k}(t) = 1$ if the individual is at site $k \in \mathcal{S}$ at time t and $P_{i,k}(t) = 0$ otherwise. We characterize the value of the states $P_{i,k}(t)$ using the following SDE with jumps:

$$dP_{i,k}(t) = dU_{i,k}(t) - dV_{i,k}(t) \quad (1)$$

where $U_{i,k}(t)$ and $V_{i,k}(t)$ are counting processes recording the events of individual i arriving at and leaving site $k \in \mathcal{S}$, respectively. Moreover, we define their intensity functions as follows:

$$\begin{aligned} P(dU_{i,k}(t) = 1 | \mathcal{H}(t)) &= \lambda_{i,k}(t) \prod_{l \in \mathcal{S}} (1 - P_{i,l}(t)) dt \\ P(dV_{i,k}(t) = 1 | \mathcal{H}(t)) &= U_{i,k}(t) v_k dt \end{aligned} \quad (2)$$

where $\lambda_{i,k}(t)$ is the rate at which individual i visits site k and $1/v_k$ is the average duration of a visit to site k . The rates $\lambda_{i,k}(t)$ and average duration $1/v_k$ for every individual and site can be configured using publicly available data as available and desired. In our simulations, we used the spatial distribution of site locations, high-resolution population density data, country-specific information about household structure, and region-specific age demographics.

Epidemiology We build on recent variations of the Susceptible-Exposed-Infected-Resistant (SEIR) compartment models that have been introduced in the context of COVID-19 modeling [33, 38]. More specifically, we define the epidemiological condition of each individual $i \in \mathcal{V}$ using the indicator state variables $\mathbb{S}(t) = \{S_i(t), E_i(t), I_i^a(t), I_i^p(t), I_i^s(t), H_i(t), R_i(t), D_i(t)\}_{i \in \mathcal{V}}$ with each $\in \{0, 1\}$, whose meaning is specified in Table 1. Their values and state transitions are characterized by the following SDEs with jumps:

$$\begin{aligned} dS_i(t) &= -S_i(t)dN_i(t) \\ dE_i(t) &= dN_i(t) - dM_i(t) \\ dI_i^a(t) &= a_i dM_i(t) - dR_i^a(t) \\ dI_i^p(t) &= (1 - a_i)dM_i(t) - dW_i(t) \\ dI_i^s(t) &= dW_i(t) - (1 - b_i)dR_i^s(t) - b_i dZ_i(t) \\ dR_i(t) &= a_i dR_i^a(t) + (1 - a_i)dR_i^s(t) \\ dH_i(t) &= h_i I_i^s(t) dY_i(t) - (1 - b_i)H_i(t) dR_i^s(t) - b_i H_i(t) dZ_i(t) \\ dD_i(t) &= b_i dZ_i(t) \end{aligned} \quad (3)$$

Table 1: Epidemiological state variables $\mathbb{S}(t)$

State	Description	Infected	Contagious	Symptoms
$S_i(t)$	is susceptible	-	-	-
$E_i(t)$	is exposed	✓	-	-
$I_i^a(t)$	is asymptomatic, mild course of disease	✓	✓	-
$I_i^p(t)$	is pre-symptomatic, progresses to $I_i^s(t)$ later	✓	✓	-
$I_i^s(t)$	is symptomatic	✓	✓	✓
$H_i(t)$	is hospitalized	✓	✓	✓
$R_i(t)$	is resistant & recovered	-	-	-
$D_i(t)$	has died	-	-	-

where $a_i \sim \text{Bern}(\alpha_a)$ indicates whether an infected individual i is asymptomatic, $h_i \sim \text{Bern}(\alpha_h)$ whether they eventually require hospitalization, and $b_i \sim \text{Bern}(\alpha_b)$ whether they eventually die.

The counting processes $\mathbb{C}(t) = \{N_i(t), M_i(t), R_i^a(t), R_i^s(t), W_i(t), Y_i(t), Z_i(t)\}_{i \in \mathcal{V}}$ model all the state transitions. For individual i , the first arrivals of the processes model the transition of i from susceptible to exposed ($N_i(t)$), from exposed to infected ($M_i(t)$), from presymptomatic infected to symptomatic infected ($W_i(t)$), from asymptomatic infected to resistant ($R_i^a(t)$), from symptomatic infected to resistant ($R_i^s(t)$), from symptomatic infected to hospitalized ($Y_i(t)$), and from symptomatic infected to dead ($Z_i(t)$).

At the core of our modeling framework, we define the conditional intensity function $\lambda_i^*(t)$ of the exposure counting process $N_i(t)$ as

$$\lambda_i^*(t) = \sum_{k \in \mathcal{S}} \beta_k P_{i,k}(t) \sum_{j \in \mathcal{V} \setminus \{i\}} \int_{t-\delta}^t K_{j,k}(\tau) e^{-\gamma(t-\tau)} d\tau \quad (4)$$

where

$$K_{j,k}(\tau) = (I_j^s(\tau) + I_j^p(\tau) + \mu I_j^a(\tau)) P_{j,k}(\tau)$$

and $P(dN_i(t) = 1 | \mathcal{H}(t)) = \lambda_i^*(t) dt$. In the above, we have that

- (i) $\beta_k \geq 0$ is the transmission rate due to presymptomatic and symptomatic individuals currently visiting site k .³
- (ii) $\mu \in [0, 1]$ is the relative transmission rate of asymptomatic compared to (pre-)symptomatic individuals.
- (iii) $\int_{t-\delta}^t K_{j,k}(\tau) e^{-\gamma(t-\tau)} d\tau$ accounts for environmental transmission, *i.e.*, it accounts for the fact that the virus may survive for some period of time on surfaces or in the air after an infected individual has left a site [39].

The exposure intensity in Eq. 4 models that an individual's instantaneous rate of exposure increases by a constant site-specific transmission rate β_k when in contact with another infectious individual at a site, in addition to capturing environmental transmission. The exposure rate of each individual i only depends on the individual's contacts, not the contacts of others. Infections within households can be characterized by adding an additional additive rate $\lambda_{\mathcal{H}(i)}(t)$ with transmission rate ξ to $\lambda_i^*(t)$, as outlined in Appendix A.

As commonly done in this context [40, 41], the time-to-event distributions of the remaining mobility-independent counting processes $M_i(t)$, $R_i^a(t)$, $R_i^s(t)$, $W_i(t)$, $Y_i(t)$, and $Z_i(t)$ are modeled as log-normal ($\log \mathcal{N}$), starting at the time $E_i(t)$, $I_i^p(t)$, $I_i^a(t)$ or $I_i^s(t)$ become one, respectively. Their parameters are fixed based on recent estimates by COVID-19 literature and summarized in Table 2.

³Depending on the availability of labeled and unlabeled data, one may consider different settings, such as all sites sharing the same parameter β or sites of the same category c sharing β_c .

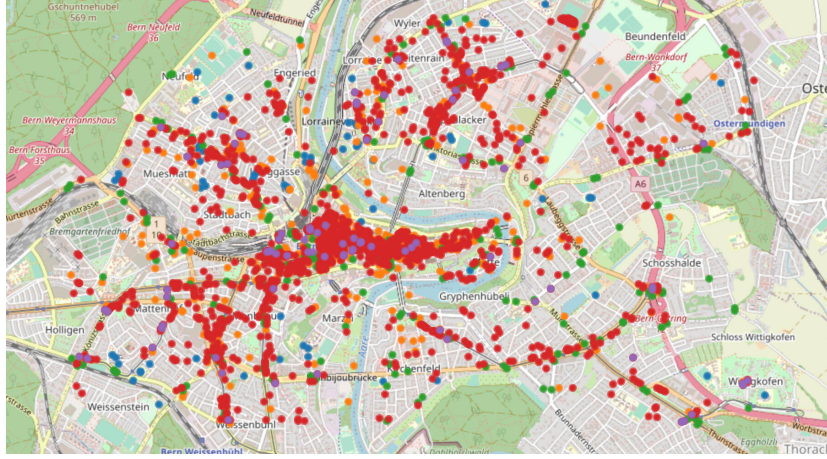


Figure 1: **Site locations by category in the mobility model of Bern, Switzerland.** Circles depict schools and research institutes (blue), social places (orange), bus stops (green), workplaces (red), and supermarkets (purple).

Containment measures In the above context, we can characterize a variety of containment measures. These may range from less restrictive (*e.g.*, isolating individuals who have tested positive) to more restrictive (*e.g.*, implementing a state of “lockdown” for the entire population via curfews). The effect of social distancing and quarantine can be faithfully characterized by reducing the rates $\lambda_{i,k}(t)$ at which individuals visit sites in the mobility model by a fraction ρ . Business restrictions can be characterized by reducing (*e.g.*, hygienic measures) or setting to zero (*e.g.*, closures) the transmission rates β_k of the sites individuals visit. In both cases, the measures lead to a reduction of the conditional intensities $\lambda_i^*(t)$ of the exposure counting processes $N_i(t)$, possibly dynamically.

Testing Our model maintains a queue Q_{test} of individuals to be tested. Over time, individuals are added to the queue according to a testing policy $\pi_{\text{test}}(t)$, *e.g.*, testing only symptomatic or vulnerable people. Individuals from the queue are tested at a rate $\lambda_{\text{test}}(t)$, which can be chosen to match location specific testing statistics. The outcome of tests is only known after a reporting delay Δ_{test} .

Formally, let the counting process $T(t)$ record the number of known test outcomes by time t , and let $T_i^+(t)$ and $T_i^-(t)$ be the number of times an individual $i \in \mathcal{V}$ has been tested positive and negative, respectively, by time t . Then, we characterize the state variables $T_i^+(t)$ and $T_i^-(t)$ using the following SDEs with jumps:

$$\begin{aligned} dT_i^+(t) &= [E_i(t) + I_i^a(t) + I_i^p(t) + I_i^s(t)] d_i(t) dT(t + \Delta_{\text{test}}) \\ dT_i^-(t) &= [S_i(t) + R_i(t)] d_i(t) dT(t + \Delta_{\text{test}}) \end{aligned} \quad (5)$$

where $P(dT(t) = 1 | \mathcal{H}(t)) = \lambda_{\text{test}}(t)dt$ and $d_i(t) \in \{0, 1\} \sim \pi_{\text{test}}(t)$ indicates whether i is tested at time t according to the policy.

Contact tracing When an individual i is tested positive, individuals previously in contact with i could be isolated or advised to seek testing. Under our model, a location-based contact tracing system records the times when an individual i checks in at different sites $k \in \mathcal{S}$, *i.e.*, it observes $P_{i,k}(t)$. Thus, it can identify the set of individuals $\mathcal{C}_i(t_0, t_f)$ who had contact with individual i during a time window $[t_0 - \delta, t_f]$ at any possible site $k \in \mathcal{S}$, where δ accounts for environmental transmission [39], analogous to the exposure rates λ_i^* in Eq. 4. By contrast, a proximity-based tracing system would be unable to account for environmental transmission, only identifying physically close contacts $\mathcal{C}'_i(t_0, t_f)$ of individual i during a time window $[t_0, t_f]$. Once a tracing system has identified contacts $\mathcal{C}_i(t_0, t_f)$ or $\mathcal{C}'_i(t_0, t_f)$, different contact tracing policies could be implemented in various contexts. Amongst many possible policies, we study the strategy of allocating tests

based on the empirical exposure probability of contacts of an infectious person, which can be estimated using our framework. Refer to Appendix B for details.

3 Sampling Algorithm

In this section, we describe how to generate exact simulations of the individual epidemiological states $\mathbb{S}(t)$ under social distancing measures, business restrictions, and a testing and tracing strategy, given initial conditions $\mathbb{S}(0)$ as well as fixed or a priori simulated mobility patterns $P_{i,k}(t)$ over a time horizon $t \in [0, t_{\max}]$.

Algorithmic backbone First, note that the epidemiological state variables $\mathbb{S}(t)$ in the model SDEs (3) change at – and only change at – *events* of the counting processes $\mathbb{C}(t)$. Since these state transitions happen at specific points in continuous time, all state variables $\mathbb{S}(t)$ are *constant between two consecutive events* when considering all event times of $\mathbb{C}(t)$ on *one* timeline. This leads us to the backbone principle for generating realizations of our model. We initialize the state variables $\mathbb{S}(0)$, compute the next time of state transition for each $i \in \mathcal{V}$, and push these transition events onto *one* single temporally-sorted priority queue Q , simultaneously tracking the next events for *all* individuals of the model. Then, the algorithm loops repeatedly through (i) popping the next event e from Q ; (ii) updating the state of individual i associated with e ; (iii) sampling the next time t of state transition e' for i ; and (iv) pushing e' to Q with priority t .

As explained in Section 2, we fix the time-to-event distributions of all non-exposure processes $\mathbb{C}(t) \setminus \{N_i(t)\}_{i \in \mathcal{V}}$ to independent, easy-to-sample distributions as estimated by clinical COVID-19 literature. Thus, sampling the first event time of $N_i(t)$, *i.e.*, the exposure time, is the central difficulty as the rates $\lambda_i^*(t)$ interact with all other state variables $\mathbb{S}(t)$ through the mobility model $P_{i,k}(t)$.

Sampling exposure times To sample the exposure event time of individual i , we need to sample the time to the next event of $N_i(t)$ with rate $\lambda_i^*(t)$. To this end, we first decompose the intensity $\lambda_i^*(t)$ into a sum of contributions $\lambda_{j \rightarrow i}^*(t)$ caused by other individuals j

$$\lambda_i^*(t) = \sum_{j \in \mathcal{V} \setminus \{i\}} \sum_{k \in \mathcal{S}} \beta_k P_{i,k}(t) \int_{t-\delta}^t K_{j,k}(\tau) e^{-\gamma(t-\tau)} d\tau =: \sum_{j \in \mathcal{V} \setminus \{i\}} \lambda_{j \rightarrow i}^*(t), \quad (6)$$

where the last summation over $j \in \mathcal{V} \setminus \{i\}$ is *sparse* as it effectively indexes over *contacts* of individuals i at times in the future, since $\lambda_{j \rightarrow i}^*(t) = 0$ when i and j are not in contact directly or j left site $k \in \mathcal{S}$ more than δ -time before i arrived.

By Eq. 6, the counting process $N_i(t)$ can be seen as a *superposition* of several processes $N_{j \rightarrow i}(t)$ with rates $\lambda_{j \rightarrow i}^*(t)$, *i.e.*, $N_i(t) = \sum_{j \in \mathcal{V} \setminus \{i\}} N_{j \rightarrow i}(t)$. Hence, the *first* arrival of the counting process $N_i(t)$ is the *minimum* of the next arrival times of all $N_{j \rightarrow i}(t)$ [19, 42]. Since we have the temporally-sorted priority queue Q in place, we can use its ordering invariant to process valid exposure events of individuals on the fly. Whenever an individual j becomes *infectious* – either via $I_j^a = 1$ or $I_j^p = 1$ – we sample the next exposure event that j *causes* for every individual i in contact with j in the future at rate $\lambda_{j \rightarrow i}^*(t)$, and push the events onto Q . When an exposure event e for individual i is popped from Q in step (i), we check that e is the *first* exposure of individual i by verifying $S_i(t) = 0$, discarding later exposure events for i that get popped from Q by finding $S_i(t) = 1$.

We can sample the next event time of $N_{j \rightarrow i}(t)$ after time t' by *thinning* [19], *i.e.*, adding up $\tau \sim \text{Expo}(\lambda_{j \rightarrow i}^{\max})$ to t' until stopping with probability $\lambda_{j \rightarrow i}^*(t')/\lambda_{j \rightarrow i}^{\max}$, where $\lambda_{j \rightarrow i}^{\max}$ is an upper bound on $\lambda_{j \rightarrow i}^*(t)$. By Eq. 6, we have $\lambda_{j \rightarrow i}^{\max} = \max_{k \in \mathcal{S}} \{\beta_k(1 - \exp(-\gamma\delta))/\gamma\} \geq \lambda_{j \rightarrow i}^*(t) \forall t \in \mathbb{R}_+$. Note that $\lambda_{j \rightarrow i}^*(t)$ is non-zero only when j has infectious contact with i , either by meeting i at a site $k \in \mathcal{S}$ or by leaving k less than δ -time before i arrives. We skip zero-intensity windows whenever reaching $\lambda_{j \rightarrow i}^*(t) = 0$ during thinning, which is sound by viewing $N_{j \rightarrow i}(t)$ itself as a superposition of counting processes, one for each interval of non-zero intensity, and skipping their initial zero-rate periods by the memoryless property.⁴

⁴If $T \sim \text{Expo}(\lambda)$, then $P(T \geq t + s \mid T \geq s) = P(T \geq t)$.

Thinning While the above handles the generation of exposure events, an individual j could recover before all exposures caused by j occurred, *i.e.*, got popped from Q . If j recovers, *i.e.* $R_j(t) = 1$, then $\lambda_{j \rightarrow i}^*(t) = 0$ in Eq. 6 at the time of this event, which was pushed to Q earlier when $\lambda_{j \rightarrow i}^*(t) > 0$. By the principle of thinning, such an exposure event has to be discarded, which can be easily verified on the fly by checking $R_j(t) \neq 1$ at the time of exposure. Lastly, note that measures such as social distancing – sparsifying $P_{i,k}(t)$ – or business restrictions – reducing β_k – always *reduce* the rates $\lambda_{j \rightarrow i}^*(t)$ in Eq. 6, and can thus also be implemented using thinning, *i.e.*, rejecting affected exposure events with some probability.

Queue-based sampling algorithm Combining our considerations above, we arrive at an efficient sampling procedure using a single temporally-sorted priority queue Q for generating sound simulations of the model SDEs. The pseudocode for the overall sampling algorithm is provided in Algorithms 2 and 3 in the appendix.

While a formal analysis of its computational complexity depends on many moving parts, we have empirically found that our sampling algorithm scales to regions with hundreds of thousands of inhabitants. For example, an 8-week simulation of Tübingen under “lockdown” interventions with 90,546 inhabitants and 1,472 sites (see Section 6, Figure 2) takes $20.7 \pm (4.6)$ minutes on a 2020 MacBook Air. Moreover, note that random rollouts can be embarrassingly parallelized.

4 Parameter Estimation

Given a fixed set of individual mobility traces $P_{i,k}(t)$ for $t \in [0, t_{\max}]$ over t_{\max} days as well as initial conditions $\mathbb{S}(0)$, we build upon the sampling algorithm introduced in Section 3 and apply Bayesian optimization (BO) to estimate the model parameters $\theta = \{\{\beta_k\}, \xi, \rho\}$ using real COVID-19 case data in a given region [20, 21].

Bayesian optimization BO defines a *probabilistic surrogate model* p of a black-box objective f to be maximized, which is however only observed at a set \mathcal{D} of noisy evaluations. As commonly done, we choose p to be a Gaussian process (GP) posterior. An *acquisition function* defined over p guides the strategy of where to next evaluate f . BO then amounts to repeatedly evaluating f at arguments proposed by the acquisition function over p , and updating p with the newly observed evaluations of f [20, 43].

Black-box model We define the black-box functions observed from our model as the *mean number of positive cases at time t*

$$g_t(\theta) = \mathbb{E}_{\mathcal{T} \sim \mathfrak{T}(\theta)} \left[\sum_{T_i^+ \in \mathcal{T}} T_i^+(t) \right] \approx \frac{1}{J} \sum_{j=1}^J \sum_{T_i^+ \in \mathcal{T}^{(j)}} T_i^+(t) \quad (7)$$

with free exposure parameters θ and $\{T_i^+(t)\} =: \mathcal{T}^{(j)} \sim \theta$ being sets of state variables indicating a positive test, sampled independently and randomly from the model under θ . Observations of $g_t(\theta)$ are stochastic and can be seen as noisy, as we use mean positive cases of J random realizations to approximate the expectation.

Realizations $\mathcal{T}^{(j)}$ are stochastic not only due to the counting processes, but in absence of real mobility traces also due to random seeds $\mathbb{S}(0)$ and synthetic $P_{i,k}(t)$, independently simulated for each rollout. We will view the t_{\max} stochastic functions g_t as one vector-valued black-box function defined as $\mathbf{g}(\theta) \in \mathbb{R}^{|t_{\max}|}$ with $\mathbf{g}(\theta)_t := g_t(\theta)$.

Objective function The objective we aim to *minimize* in our setting is the *sum of daily squared errors of cumulative positive cases* between the model predictions and real COVID-19 case data over a horizon of t_{\max} days. This allows us to form a link between the spatiotemporal states of each individual in the model and aggregate longitudinal case data. The squared error has been previously considered in parameter estimation for black-box models [44].

Algorithm 1 Parameter estimation using Bayesian optimization

Input: Black-box simulator $\mathbf{g}(\theta)$, parameter domain $\text{dom}(\theta)$, time horizon t_{\max} , case data c_t^{true} , hyperparameters N, M, J

- 1: $s(\mathbf{x}) := -\sum_{t=1}^{t_{\max}} (c_t^{\text{true}} - \mathbf{x}_t)^2$
- 2: $\theta_{1:M} \leftarrow$ first M points of Sobol sequence [50] in $|\theta|$ dims., scaled to $\text{dom}(\theta)$
- 3: $\mathcal{D} \leftarrow \emptyset$
- 4: **for** $i \in [M]$ **do** ▷ Quasi-random exploration for initialization
- 5: Obtain noisy sim. evaluation $\mathbf{g}(\theta_i)$ from J random roll-outs
- 6: $\mathcal{D} \leftarrow \mathcal{D} \cup \{(\theta_i, \mathbf{g}(\theta_i))\}$
- 7: **while** $|\mathcal{D}| \leq N$ **do** ▷ Bayesian Optimization
- 8: $p(\mathbf{g}(\theta)) \mid \mathcal{D} \leftarrow \text{GP}(\mathcal{D})$
- 9: $\theta^* \leftarrow \arg \max_{\theta' \in \text{dom}(\theta)} \text{KG}(\theta')$
- 10: Obtain noisy sim. evaluation $\mathbf{g}(\theta^*)$ from J random roll-outs
- 11: $\mathcal{D} \leftarrow \mathcal{D} \cup \{(\theta^*, \mathbf{g}(\theta^*))\}$
- 12: **return** $\arg \max_{(\theta, \mathbf{g}(\theta)) \in \mathcal{D}} s(\mathbf{g}(\theta))$

Let c_t^{true} be the cumulative number of real COVID-19 cases at the end of day t as provided by the national authorities [45, 46]. Then, our objective f to be *maximized* is a composition of the negative squared error score s and the black-box function \mathbf{g} from above.

$$f(\theta) = s(\mathbf{g}(\theta)) = -\sum_{t=1}^{t_{\max}} \left(c_t^{\text{true}} - g_t(\theta)\right)^2 \quad (8)$$

The composition of f allows for greater sample efficiency since the surrogate model p is able to learn the black-box function \mathbf{g} directly, which has recently shown to bear great performance boosts [43, 44].

Knowledge gradient Since evaluations of f are inherently noisy, we use the knowledge gradient acquisition function (KG) [47, 48] to navigate parameter proposals, which often shows favorable performance in noisy settings [43, 49]. KG quantifies the expected increase in the maximum of the posterior mean of p after an observation at a given θ . The KG of measuring at θ is defined as

$$\text{KG}(\theta) := \mathbb{E}_{\mathbf{y} \sim p(\mathbf{g}(\theta) \mid \mathcal{D})} \left[\mu^*(\mathcal{D} \cup \{(\theta, \mathbf{y})\}) - \mu^*(\mathcal{D}) \right] \quad (9)$$

$$\mu^*(\cdot) = \max_{\theta' \in \text{dom}(\theta)} \mathbb{E} \left[s(\mathbf{g}(\theta')) \mid \cdot \right] \quad (10)$$

where $\mu^*(\mathcal{D} \cup \{(\theta, \mathbf{y})\})$ and $\mu^*(\mathcal{D})$ denote the maxima of the conditional means of the objective f given the observations $\mathcal{D} \cup \{(\theta, \mathbf{y})\}$ and \mathcal{D} , respectively, under the surrogate model p .

Combining the above into the BO paradigm, the overall parameter estimation procedure is summarized in Algorithm 1.

5 Experimental Design

We showcase our modeling framework on both rural and urban areas in Germany and Switzerland spanning a wide range of infection levels until July 2020. More specifically, we experiment with two cities and one district (Landkreis) in Germany—Tübingen, Kaiserslautern and the Landkreis of Rheingau-Taunus—and two cities and one state (Canton) in Switzerland—Bern, Locarno, and the Canton of Jura. See Table 4 in the appendix for details.

5.1 Scenarios

We use the sampling algorithm for our model derived in Section 3 to simulate the spread of COVID-19 under a variety of interventions in two different scenarios:

- **Scenario A (*Initially uncontrolled*):** *Early stage of the outbreak. After a reaction delay, governments aim to globally contain and suppress infections in the population. At the time of intervention, there is already a significant number of infections.*

Setup: We simulate the spread of COVID-19 from the day when a given region had five to ten confirmed cases, typically in early March, until the end of the “lockdown” period⁵, assuming that measures are in place *only* during the “lockdown” period. Refer to Appendix C for details on state initialization in this scenario.

- **Scenario B (*Continual suppression*):** *Later stage of the epidemic. Measures taken by the governments ended the first wave of infections. Local outbreaks occur due to imported cases, e.g., from visits to other regions. Contact tracing and localized interventions are employed as more fine-grained tools.*

Setup: We simulate the spread of COVID-19 for 120 days assuming *five imported cases per week per 100,000 inhabitants* in expectation.

5.2 Mobility traces

For lack of real check-in traces $P_{i,k}(t)$ available to us, we utilize real demographic and geolocation data to set the values of the intensities $\lambda_{i,k}(t)$ and v_k in the mobility model of Section 2, which we then use to generate synthetic check-in traces.

Demographic data We use high-resolution population density data provided by *Facebook Data for Good* [54] to build a region-specific population model. A respective area population \mathcal{V} is proportionally assigned to equally-sized tiles according to the population density in each tile. Individuals belong to one of six age groups according to the real demographics of the region, matching the age groups of the COVID-19 case data [45, 46]. Ultimately, these individuals are placed in households of sizes one to five according to their age categories and country-specific household structure [55, 56], and then are located uniformly at random within their tile.

Geolocation data To obtain relevant site locations in our regions of interest, we use geolocation data provided by *OpenStreetMap* [57]. Specifically, we retrieve the location of all sites \mathcal{S} in five site categories: *education* (schools, universities, research institutes), *social* (restaurants, cafés, bars), *transportation* (bus stops), *work* (offices, shops), and *groceries* (supermarkets, convenience stores).

Setting the intensity values We assume each individual i visits only a constrained set of unique sites $\mathcal{S}_i \subset \mathcal{S}$, which are picked with probability inversely proportional to the squared distance from their homes. This reflects the fact that individuals typically study or work at only one place, form habits regarding the public transportation they use, and social places or supermarkets they visit. More specifically, we assume each individual visits one site for education and work, ten social sites, five sites for transportation, and two sites for groceries. Then, for each individual i and site $k \in \mathcal{S}_i$, we set the intensity $\lambda_{i,k}(t)$ to a constant value that depends on the individual’s age group and the site type. Refer to Table 3 for details. Here, we assume people of younger ages spend most of their time at school and social sites, middle-age people spend most of their time at work and elderly people have lower activity over all. Finally, we set the mean duration $1/v_k$ of any visit to a site heuristically according to the site type. In particular, we set the mean duration of visits to sites in education and work, social, transportation, and groceries to 120, 90, 12 and 30 minutes, respectively. Note that since people are neither exposed to all others at a site nor continually exposed during their visit, the visit duration in some categories are set to lower values than one would expect as real visit durations.

⁵This period of most restrictive measures started on March 23 and 16, 2020 and ended on May 3 and 10, 2020 in Germany and Switzerland, respectively [51–53].

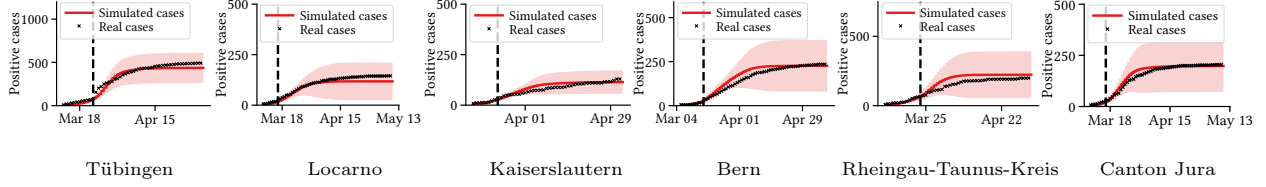


Figure 2: **Cumulative number of cases for the models of the considered regions.** The red line represents the mean cumulative number of positively tested individuals over 48 random realizations, shaded regions correspond to two times the standard deviation. The dashed line represents the start of the “lockdown” measures, and the black line the real observed cases. Averaged over days of simulation, the mean absolute error (MAE) of predicted cases ranges between 10-30 cases across the six regions.

5.3 Exposure parameter estimation

Using the procedure described in Section 4, we estimate a single transmission rate $\beta_k = \beta$ for all sites, a parameter ξ for households, and the mobility reduction ρ due to social distancing, randomly generating mobility traces $P_{i,k}(t)$ for each new rollout $\mathcal{T}^{(j)}$ of the model as described above. To this end, we use COVID-19 case data of county-level administrative regions⁶ [45, 46] over the time period described in *Scenario A* and set the mortality and hospitalization rates per age group using this data and previous studies [30]. Moreover, we emulate the corresponding business restrictions in place during the “lockdown”. For scalability reasons, we downscale the model during parameter estimation. Refer to Appendix D for additional information. Appendix E discusses when parameter estimation using downscaled models may fail.

5.4 Testing

To abstract away from testing criteria implemented in different regions, we assume that only true symptomatic individuals are registered for testing unless noted otherwise, and that the testing queue follows the first-in-first-out principle. We set the reporting delay Δ_{test} to 48 hours, accounting for both the delay in self-reporting and the testing procedure, and set the daily testing rate $\lambda_{\text{test}}(t)$ to the inverse of the maximum daily increase in positive cases in the COVID-19 data of the region. Moreover, we assume tests have perfect accuracy and positively tested individuals stop visiting sites and isolate themselves from their household.

6 Results

Using the estimated parameters β, ξ, ρ as listed in Table 5, we first validate that our model is able to faithfully characterize the real COVID-19 case data during the time period of *Scenario A*. Figure 2 summarizes the results, which show that the model consistently reproduces the longitudinal trend of real cases in all regions, and that the parameters estimated using the downscaled models are a good fit for the full-scale models used during validation. For the same setting, Figure 3 shows the distribution of secondary infections for the city of Bern. We find that the effective reproduction number R_t is pushed below the threshold of one, yet also observe that the measure of dispersion k_t is significantly lower than one during and after interventions. This suggests *overdispersion* in the number of secondary infections, *i.e.*, a situation where few individuals are likely to infect many. We found qualitatively similar results for all the other regions, which are summarized in Figures 8 and 9 in the Appendix.

Next, we use the estimated parameters to investigate the extent to which containment of the first wave of infections in *Scenario A* would have been feasible using measures with lower impact on civil liberties and the economy. To this end, we explore three counterfactual “what-if” scenarios that implement milder containment measures than those that were in place during the “lockdown” period. We show the results of an informative

⁶For cities, cases scaled proportionally to population, for lack of more available data.

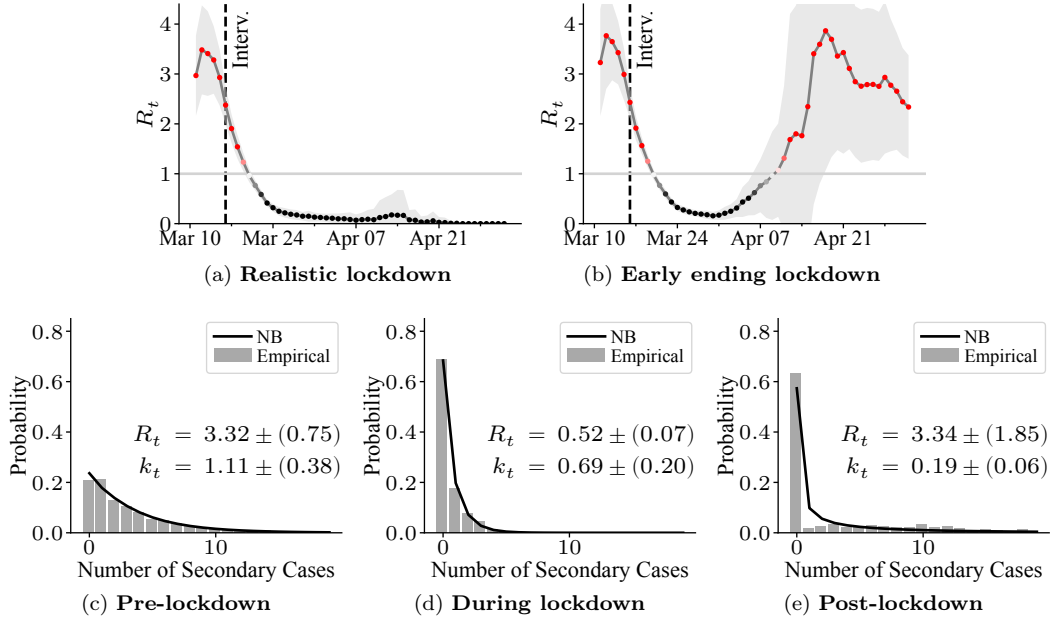


Figure 3: **Effective reproduction number in Bern (a) in the realistic lockdown scenario and (b) when restrictions are lifted after 4 weeks, where lines represent mean estimates with shaded standard deviations.** We use the approach of Athreya et al. [9], which fit a Negative-Binomial (NB) distribution to the number of secondary cases. For (b), we also report the distribution of secondary cases for pre-lockdown (c), in-lockdown (d), and post-lockdown (e) periods, where $k_t < 1$ corresponds to the overdispersion regime.

subset of the investigated regions here and refer to the longer version of the paper for a comprehensive visualization of all results.

Early ending “lockdown” We implement the same restrictive measures as in place during the “lockdown” period both in Germany and Switzerland, but reduce their duration. Figures 3 and 4a summarize the results for Bern and Rheingau-Taunus-Kreis, and Figure 10 in the Appendix for the other regions. The results suggest that, to end the first wave of infections, it should have been sufficient to maintain the “lockdown” period for just one month rather than two, whereas a period of two weeks would have been insufficient. However, in Bern as well as in all other regions except for Rheingau-Taunus-Kreis, a resurgence of infections would have occurred shortly after the end of the one month “lockdown”.

Alternating curfews for random subgroups We divide the population into K subgroups and, on each day, alternately prescribe curfews to $K - 1$ of the groups, only allowing one group to follow their usual daily activities. Figure 4b summarizes the results for Kaiserslautern and Canton Jura, and Figure 10 in the Appendix for the remaining regions. The results suggest that, as long as the number of groups $K > 2$, this containment strategy would be effective at reducing both intra- and inter-group exposure events, as argued by previous work [58, 59], and the number of infected individuals would have followed a similar course as in the “lockdown” scenario. However, for $K = 2$ groups, the results are mixed. In all the considered German towns and regions, the strategy would still be relatively successful, while in Bern and the Canton of Jura, the number of infected individuals would have constantly increased. Interestingly, this qualitative difference in outcome for $K = 2$ is reflected in the effective reproduction number shown in Figure 10, which is estimated as marginally below and above the threshold of 1, respectively.

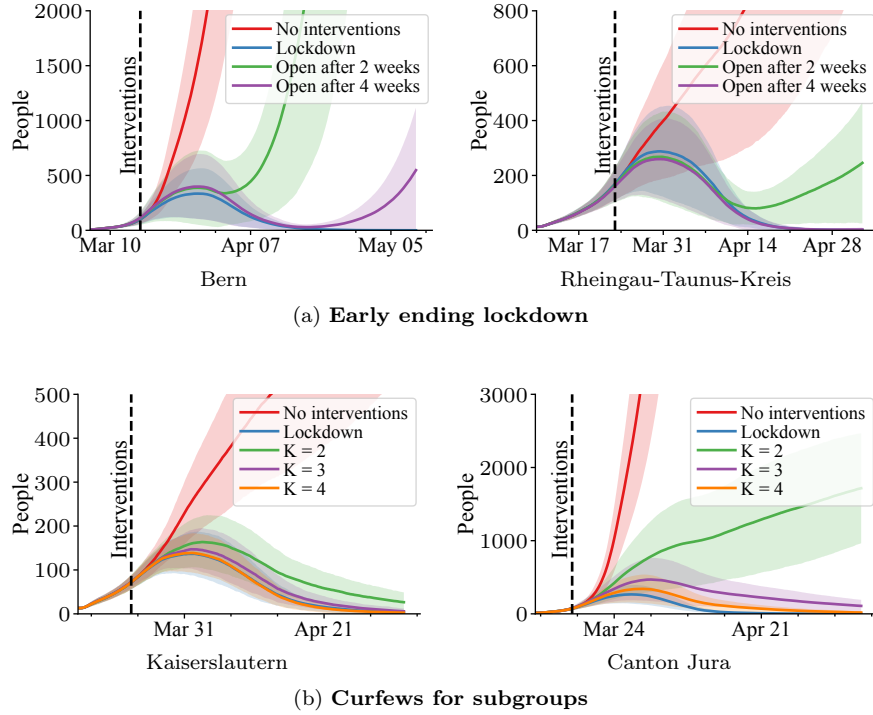


Figure 4: **Number of infected individuals in different counterfactual scenarios and regions.** The lines in panel represent the mean of the number of infected over 48 random realizations of the simulations, the shaded regions correspond to two times the standard deviation.

Social distancing of vulnerable groups In this scenario, the population over 60 years old, who typically suffers more complications from COVID-19 [45], follows the same social distancing measures that were in place during the “lockdown” period and the rest of the population follows their usual daily activities. Figure 11 in the Appendix summarizes the results, which are consistent across all considered regions. The results suggest that this containment strategy would not end the first wave of infections. In addition, we also find that such a strategy would only modestly reduce the number of hospitalizations and fatalities, questioning the effectiveness of controversial policies that initially advocated for isolating only the people who are most endangered.

Next, we focus on *Scenario B* and investigate the effectiveness of adaptive containment measures that utilize testing and contact tracing to suppress a second wave of infections.

Conditional “lockdowns” based on weekly incidence Whenever the number of new cases within 7 days exceeds the threshold of 50 per 100,000 inhabitants, we implement the same restrictive measures that were in place during the “lockdown” period in *Scenario A*. This has been the strategy in place in Germany after May 6, 2020 [60]. Figure 5 shows the number of infected people over time in single realizations of the model for Tübingen and Bern. The other regions are shown in Figure 12 in the Appendix. We observe that the repeated lifting of measures leads to fluctuations in the number of infected individuals, but the short “lockdowns” are able to quickly reduce the number of new cases below the desired threshold. While the typical length of the interventions is two weeks in Tübingen, we find that, *e.g.*, in Bern, case-conditional “lockdowns” typically last for four weeks. Qualitatively similar results were obtained across realizations for all the other regions.

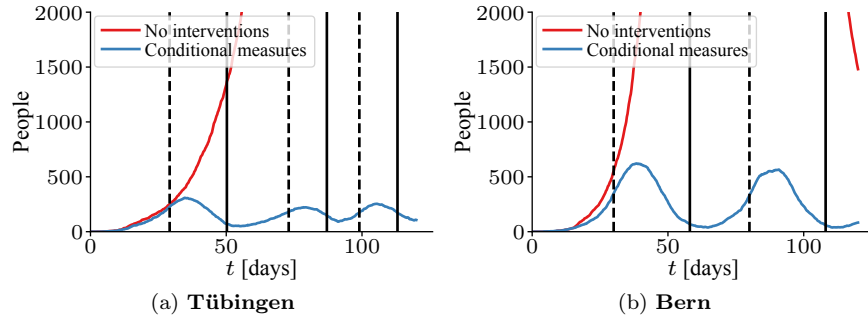


Figure 5: **Number of infected people in single simulations of the model of Tübingen and Bern under conditional “lockdowns” based on weekly incidence.** Dashed and solid vertical lines indicate beginning and ending of the “lockdowns”.

Contact tracing for isolation and testing Whenever an individual is tested positive, we use contact tracing to identify all their contacts in the 10 days leading up to the test result and isolate them from everyone for 14 days, unless mentioned otherwise. We investigate to what extent the use of rapid testing [61], *i.e.*, setting $\Delta_{\text{test}} = 3h$, or further testing of contacts⁷ can increase the effectiveness of the above basic strategy. Finally, we evaluate the effectiveness of contact tracing for isolation and testing under constraints on the compliance and an advanced testing strategy.

Figure 6 summarizes our results for Tübingen. In Figure 6a, we observe that the basic strategy, which only implements isolation of contacts, is already able to avoid a significant resurgence in infections. Moreover, the use of rapid tests and further testing of contacts provide an additional reduction on the mean and variance of infection counts across random roll-outs. Interestingly, under further testing of contacts, the number of infected people over time reaches a steady state—the effective reproduction number R_t is pushed towards one, as shown in Figure 6b. However, in this steady state, Figure 6c shows that the number of secondary infections is overdispersed with $k_t = 0.25 \pm (0.22)$, and thus a resurgence in infections may be increasingly likely due to a superspreading event. Similar findings are obtained for all other regions studied, as shown in Figure 13 in the Appendix. In further investigations, we also find that, when testing only the top 20 contacts ranked according to *empirical probability of exposure* of Appendix B, it is possible to achieve the same reduction in infections as when testing all contacts, even though the overall number of tests is reduced by 70-90% (from 47,927 to 8,821 tests in Tübingen). Finally, in Figure 6d, we observe that the effectiveness of contact tracing gradually degrades with lower compliance due to the “ x^2 problem” of adoption [38, 62], *i.e.*, two parties needing to adopt contact tracing for the infection chain to be tracked.

Narrowcasting exposure risk at sites To circumvent the “ x^2 problem”, we also test an alternative strategy called *narrowcasting* [63], where health authorities use contact tracing data of positively tested individuals to make public announcements about risk of infection, highly tailored to a location or a subset of individuals. In Appendix F, we explain how to estimate the empirical probability of exposure at a site, which help us identify potential infection hotspots. Figure 7 presents an example of narrowcasting the empirical probability of exposure in Tübingen during *Scenario A* under the estimated “lockdown” measures. Figure 15 in the Appendix presents narrowcasting for the other towns and regions.

7 Discussion

Motivated by multiple lines of evidence that strongly suggest for infection hotspots to play a key role in the transmission dynamics of COVID-19, we have introduced a spatiotemporal epidemic model that explicitly

⁷Here, we assume sufficient testing capacity for every traced contact to be tested.

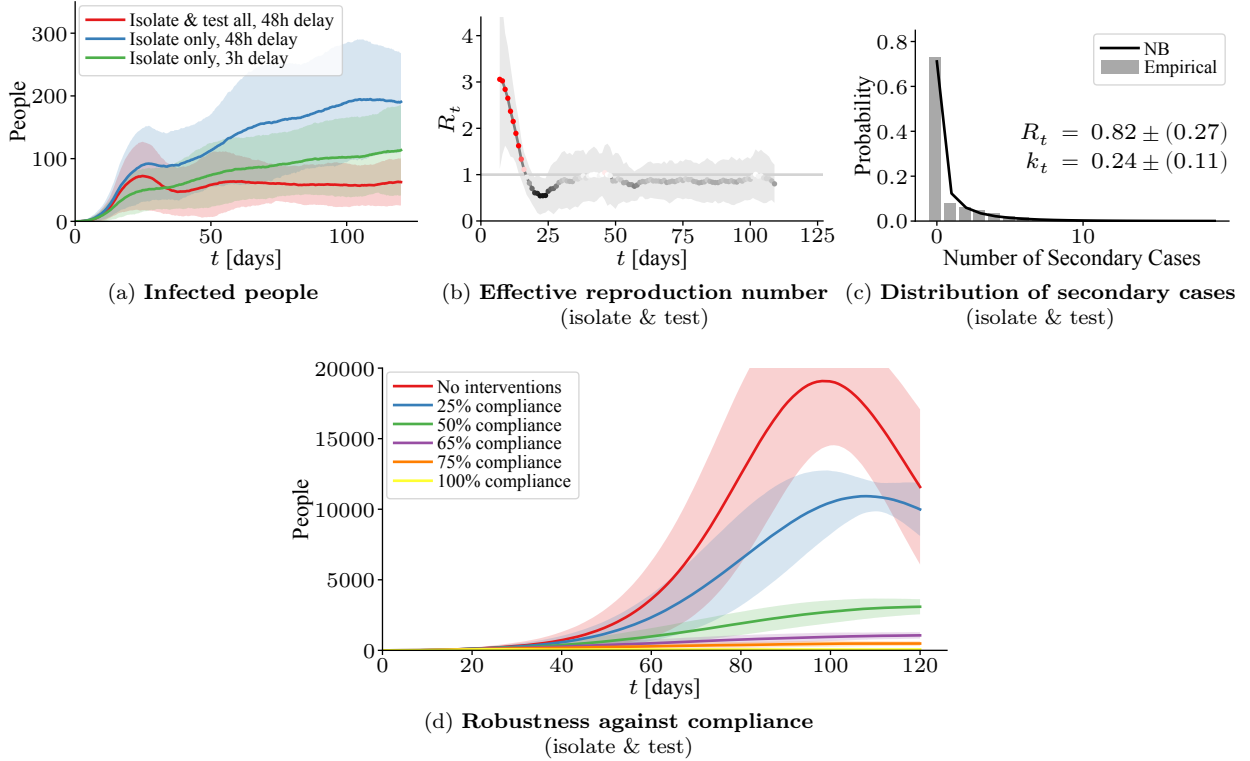


Figure 6: **Contact tracing for isolation and testing in the model of Tübingen.** Panel (a) shows the number of infected people under different strategies and reporting delays Δ_{test} . Within the testing and isolation scenario ($\Delta_{\text{test}} = 48h$), panel (b) shows the effective reproduction number, (c) the distribution of secondary cases and (d) infected people for different compliance levels.

represents sites where infections occur and hotspots may emerge. Through an extensive case study that used fine-grained demographic data, site locations, and COVID-19 data from several cities and regions in Germany and Switzerland, we have demonstrated that our model faithfully characterizes the observed longitudinal trend of COVID-19 cases. Our results reveal both qualitative and quantitative differences and similarities across geographically diverse areas spanning a wide range of case incidences, and demonstrate that our model may allow individuals and policy-makers to make more effective decisions. Importantly, our results also suggest that social distancing or contact tracing did not reduce overdispersion in the number of secondary infections, though effective containment measures would demand preventing SSEs [12, 18]. To facilitate this, we release an easy-to-use implementation of the entire framework necessary to perform experiments for any desired region.

In our work, we have used fine-grained demographic data and site locations to configure our mobility model. However, if data from contact tracing become accessible to researchers, we believe that our predictions could have lower variance and it would be possible to use our framework to identify areas with higher risk of infection in real time. Beyond legal compliance and gaining societal acceptance, the use of epidemic models with high spatiotemporal resolution such as ours should respect each individual’s privacy. In this context, it is important to highlight that, both during parameter estimation and contact tracing, we only need to compute the contact *duration* of individuals with an infected person—the identity of the infected person is not required. As a result, there are reasons to believe that such computations can be made in a decentralized and privacy-preserving manner [64, 65]. Finally, although our model has greater resolution than many of those in use today, its predictions can only be faithfully considered when being aware of the high variance observed across random realizations.

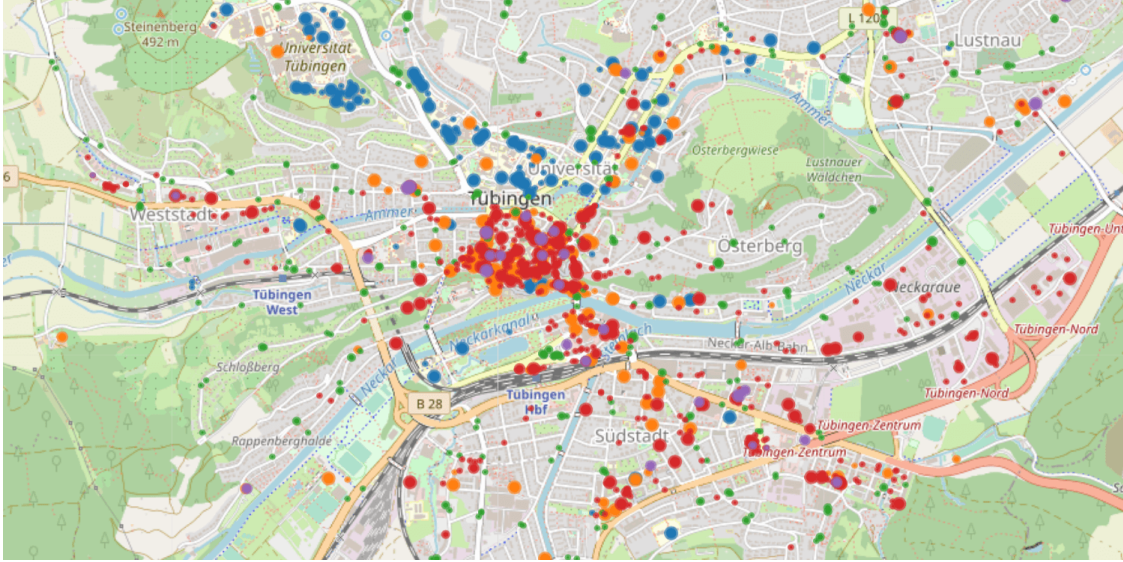


Figure 7: **Narrowcasting of exposure risk at sites during a time window of two weeks of the realistic “lockdown” scenario in Tübingen.** Circles represent sites and the size of each circle is proportional to the site’s empirical probability of exposure of a visiting individual during the time period. Colors represent site types as in Figure 1.

Acknowledgements

We thank the Robert-Koch-Institute, OpenStreetMaps and Facebook for providing data to make this work possible. We thank Brian Karrer from Facebook for his insightful comments and suggestions regarding Bayesian optimization, Kevin Murphy, Yusef Shafi and others from Google for helpful discussions, and Yannik Schaelte for useful comments on a preliminary version of this work. We thank Cansu Culha and the Stanford Future Bay Initiative as well as Pavol Harar from the University of Vienna for working with us to improve our publicly available implementation. This work was supported in part by SNSF under grant number 200021-182407.

References

- [1] World Health Organization, “Coronavirus disease (COVID-2019) situation reports,” 2020. [Online]. Available: <https://www.who.int/emergencies/diseases/novel-coronavirus-2019/situation-reports/>
- [2] Johns Hopkins University & Medicine, “Coronavirus resource center,” 2020. [Online]. Available: <https://coronavirus.jhu.edu/>
- [3] World Health Organization, “WHO Director-General’s opening remarks at the media briefing on COVID-19 - 11 March 2020,” 2020. [Online]. Available: <https://www.who.int/dg/speeches/detail/who-director-general-s-opening-remarks-at-the-media-briefing-on-covid-19---11-march-2020>
- [4] D. C. Adam *et al.*, “Clustering and superspreading potential of SARS-CoV-2 infections in Hong Kong,” *Nature Medicine*, 2020.
- [5] MSF, “Too little, too late: The unacceptable neglect of the elderly in care homes during the COVID-19 epidemic in Spain,” 2020. [Online]. Available: <https://msfcovid19.org/wp-content/uploads/2020/08/msf-report-too-little-too-late-elderly-and-covid-in-ltcf-english.pdf>

- [6] A. Endo *et al.*, “Estimating the overdispersion in COVID-19 transmission using outbreak sizes outside China,” *Wellcome Open Research*, 2020.
- [7] M. S. Lau *et al.*, “Characterizing superspreading events and age-specific infectiousness of SARS-CoV-2 transmission in Georgia, USA,” *Proceedings of the National Academy of Sciences*, vol. 117, no. 36, 2020.
- [8] T. Frieden and C. Lee, “Identifying and interrupting superspreading events—implications for control of severe acute respiratory syndrome coronavirus 2,” 2020.
- [9] S. Athreya, N. Gadhiwala, and A. Mishra, “Effective reproduction number and dispersion under contact tracing and lockdown on COVID-19 in Karnataka,” *medRxiv*, 2020. [Online]. Available: <https://www.medrxiv.org/content/early/2020/08/22/2020.08.19.20178111>
- [10] “The Korean clusters: How coronavirus cases exploded in South Korean churches and hospitals,” 2020. [Online]. Available: <https://graphics.reuters.com/CHINA-HEALTH-SOUTHKOREA-CLUSTERS/0100B5G33SB/index.html>
- [11] A. Walker *et al.*, “Genetic structure of SARS-CoV-2 reflects clonal superspreading and multiple independent introduction events, North-Rhine Westphalia, Germany, February and March 2020,” *Eurosurveillance*, vol. 25, no. 22, 2020.
- [12] M. Cevik *et al.*, “SARS-CoV-2 transmission dynamics should inform policy,” *SSRN 3692807*, 2020.
- [13] A. Hasan *et al.*, “Superspreading in early transmissions of COVID-19 in Indonesia,” *medRxiv*, 2020.
- [14] Y. Zhang *et al.*, “Evaluating transmission heterogeneity and super-spreading event of COVID-19 in a metropolis of China,” *International Journal of Environmental Research and Public Health*, 2020.
- [15] M.-d. Oh *et al.*, “Middle east respiratory syndrome coronavirus superspreading event involving 81 persons, Korea 2015,” *Journal of Korean medical science*, vol. 30, no. 11, pp. 1701–1705, 2015.
- [16] J. O. Lloyd-Smith, S. J. Schreiber, P. E. Kopp, and W. M. Getz, “Superspreading and the effect of individual variation on disease emergence,” *Nature*, vol. 438, no. 7066, pp. 355–359, 2005.
- [17] R. A. Stein, “Super-spreaders in infectious diseases,” *International Journal of Infectious Diseases*, vol. 15, no. 8, pp. e510–e513, 2011.
- [18] B. M. Althouse *et al.*, “Stochasticity and heterogeneity in the transmission dynamics of SARS-CoV-2,” *arXiv preprint arXiv:2005.13689*, 2020.
- [19] A. De, U. Upadhyay, and M. Gomez-Rodriguez, “Temporal point processes,” Technical report, Saarland University, Tech. Rep., 2019.
- [20] E. Brochu, V. M. Cora, and N. de Freitas, “A tutorial on bayesian optimization of expensive cost functions, with application to active user modeling and hierarchical reinforcement learning,” 2010.
- [21] D. R. Jones, M. Schonlau, and W. J. Welch, “Efficient global optimization of expensive black-box functions,” *Journal of Global optimization*, vol. 13, no. 4, pp. 455–492, 1998.
- [22] J. Snoek *et al.*, “Practical bayesian optimization of machine learning algorithms,” in *Advances in neural information processing systems*, 2012, pp. 2951–2959.
- [23] H. W. Hethcote, “The mathematics of infectious diseases,” *SIAM review*, vol. 42, no. 4, pp. 599–653, 2000.
- [24] A. W. Roddam, “Mathematical Epidemiology of Infectious Diseases: Model Building, Analysis and Interpretation,” *International Journal of Epidemiology*, 2001.

- [25] H. J. Ahn and B. Hassibi, “Global dynamics of epidemic spread over complex networks,” in *CDC*, 2013.
- [26] E. Cator and P. Van Mieghem, “Second-order mean-field susceptible-infected-susceptible epidemic threshold,” *Physical review E*, 2012.
- [27] D. Chakrabarti *et al.*, “Epidemic thresholds in real networks,” *ACM TISSEC*, 2008.
- [28] P. Van Mieghem, “The N-intertwined SIS epidemic network model,” *Computing*, 2011.
- [29] P. Van Mieghem, J. Omic, and R. Kooij, “Virus spread in networks,” *IEEE/ACM TON*, 2009.
- [30] N. M. Ferguson *et al.*, “Impact of non-pharmaceutical interventions (NPIs) to reduce COVID-19 mortality and healthcare demand,” *London: Imperial College COVID-19 Response Team, March*, vol. 16, 2020.
- [31] S. M. Moghadas *et al.*, “Projecting hospital utilization during the COVID-19 outbreaks in the United States,” *PNAS*, 2020.
- [32] C. R. Wells *et al.*, “Impact of international travel and border control measures on the global spread of the novel 2019 coronavirus outbreak,” *PNAS*, 2020.
- [33] R. Li *et al.*, “Substantial undocumented infection facilitates the rapid dissemination of novel coronavirus (SARS-CoV2),” *Science*, 2020.
- [34] L. Di Domenico *et al.*, “Expected impact of school closure and telework to mitigate COVID-19 epidemic in France,” 2020.
- [35] R. Herbrich, R. Rastogi, and R. Vollgraf, “Crisp: A probabilistic model for individual-level COVID-19 infection risk estimation based on contact data,” 2020.
- [36] A. J. Kucharski *et al.*, “Effectiveness of isolation, testing, contact tracing, and physical distancing on reducing transmission of SARS-CoV-2 in different settings: a mathematical modelling study,” *The Lancet Infectious Diseases*, 2020.
- [37] A. Aleta *et al.*, “Modelling the impact of testing, contact tracing and household quarantine on second waves of COVID-19,” *Nature Human Behaviour*, 2020.
- [38] L. Ferretti *et al.*, “Quantifying dynamics of SARS-CoV-2 transmission suggests that epidemic control and avoidance is feasible through instantaneous digital contact tracing,” *Science*, 2020.
- [39] N. van Doremalen *et al.*, “Aerosol and surface stability of HCoV-19 (SARS-CoV-2) compared to SARS-CoV-1,” *medRxiv*, 2020.
- [40] S. A. Lauer *et al.*, “The incubation period of coronavirus disease 2019 (COVID-19) from publicly reported confirmed cases: Estimation and application,” *Annals of Internal Medicine*, 2020.
- [41] N. M. Linton *et al.*, “Incubation period and other epidemiological characteristics of 2019 novel coronavirus infections with right truncation,” *Journal of Clinical Medicine*, vol. 9, no. 2, 2020.
- [42] O. O. Aalen, Ø. Borgan, and H. K. Gjessing, *Survival and Event History Analysis*. Springer New York, 2008.
- [43] M. Balandat *et al.*, “Botorch: Programmable bayesian optimization in pytorch,” 2019.
- [44] R. Astudillo and P. I. Frazier, “Bayesian optimization of composite functions,” 2019.
- [45] Robert Koch-Institut (RKI), “COVID-19 data set,” 2020. [Online]. Available: <https://npgeo-corona-npgeo-de.hub.arcgis.com/datasets/>

- [46] Bundesamt für Gesundheit, Schweiz, “BAG COVID-19 situation summary,” 2020. [Online]. Available: <https://www.bag.admin.ch/bag/en/home/krankheiten/ausbrueche-epidemien-pandemien/aktuelle-ausbrueche-epidemien/novel-cov/situation-schweiz-und-international.html>
- [47] P. I. Frazier, W. B. Powell, and S. Dayanik, “A knowledge-gradient policy for sequential information collection,” *SIAM J. Control Optim.*, vol. 47, no. 5, p. 2410–2439, Sep. 2008.
- [48] J. Wu and P. Frazier, “The parallel knowledge gradient method for batch bayesian optimization,” in *Advances in Neural Information Processing Systems 29*. Curran Associates, Inc., 2016, pp. 3126–3134.
- [49] P. I. Frazier, “A tutorial on bayesian optimization,” 2018.
- [50] I. Sobol, “On the distribution of points in a cube and the approximate evaluation of integrals,” *USSR Computational Mathematics and Mathematical Physics*, vol. 7, no. 4, 1967.
- [51] Land Baden-Württemberg, “Verordnung der Landesregierung über infektionsschützende Massnahmen gegen die Ausbreitung des Virus SARS-Cov-2 (Corona-Verordnung),” 2020. [Online]. Available: <https://www.baden-wuerttemberg.de/de/service/aktuelle-infos-zu-corona/aktuelle-corona-verordnung-des-landes-baden-wuerttemberg/>
- [52] Bundesländer der Bundesrepublik Deutschland, “Corona-Regelungen in den Bundesländern,” 2020. [Online]. Available: <https://www.bundesregierung.de/breg-de/themen/coronavirus/corona-bundeslaender-1745198>
- [53] Der Schweizerische Bundesrat, “Verordnung 2 über Massnahmen zur Bekämpfung des Coronavirus (COVID-19) (COVID-19-Verordnung 2),” 2020. [Online]. Available: <https://www.admin.ch/opc/de/classified-compilation/20200744/index.html>
- [54] “Facebook Data for Good,” 2020. [Online]. Available: <https://dataforgood.fb.com>
- [55] Statistisches Bundesamt, Deutschland, “Households, by type of household. Long-term series with annual data from 1961,” 2020. [Online]. Available: <https://www.destatis.de/EN/Themes/Society-Environment/Population/Households-Families/Tables/lrbev05.html>
- [56] Bundesamt für Statistik, Schweiz, “Households,” 2020. [Online]. Available: <https://www.bfs.admin.ch/bfs/de/home/statistiken/bevoelkerung/stand-entwicklung/haushalte.html>
- [57] “OpenStreetMap,” 2020. [Online]. Available: <https://www.openstreetmap.org/>
- [58] O. Karin *et al.*, “Adaptive cyclic exit strategies from lockdown to suppress COVID-19 and allow economic activity,” *medRxiv*, 2020.
- [59] D. Meidan *et al.*, “An alternating lock-down strategy for sustainable mitigation of COVID-19,” *arXiv preprint arXiv:2004.01453*, 2020.
- [60] Bundesregierung Deutschland, “Telefonschaltkonferenz der Bundeskanzlerin mit den Regierungschefinnen und Regierungschefs der Länder am 6. Mai 2020,” 2020. [Online]. Available: <https://www.bundesregierung.de/resource/blob/973812/1750986/fc61b6eb1fc1d398d66cfea79b565129/2020-05-06-mpk-beschluss-data.pdf>
- [61] European Center for Disease Prevention and Control, “An overview of the rapid test situation for COVID-19 diagnosis in the EU/EEA,” 2020. [Online]. Available: <https://www.ecdc.europa.eu/sites/default/files/documents/Overview-rapid-test-situation-for-COVID-19-diagnosis-EU-EEA.pdf>
- [62] J. Langford, “Critical issues in digital contract tracing,” 2020. [Online]. Available: <https://hunch.net/?p=13762603>

- [63] J. Chan *et al.*, “Pact: Privacy sensitive protocols and mechanisms for mobile contact tracing,” *arXiv preprint arXiv:2004.03544*, 2020.
- [64] M. Nanni *et al.*, “Give more data, awareness and control to individual citizens, and they will help COVID-19 containment,” 2020.
- [65] C. Troncoso *et al.*, “Decentralized privacy-preserving proximity tracing,” 2020. [Online]. Available: <https://github.com/DP-3T/documents/blob/master/DP3T%20White%20Paper.pdf>
- [66] World Health Organization, “Report of the WHO-China joint mission on coronavirus disease 2019 (COVID-19),” 2020. [Online]. Available: <https://www.who.int/docs/default-source/coronaviruse/who-china-joint-mission-on-covid-19-final-report.pdf>
- [67] X. He *et al.*, “Temporal dynamics in viral shedding and transmissibility of COVID-19,” *Nature Medicine*, vol. 26, no. 5, pp. 672–675, May 2020.
- [68] R. Woelfel *et al.*, “Clinical presentation and virological assessment of hospitalized cases of coronavirus disease 2019 in a travel-associated transmission cluster,” *medRxiv*, 2020.
- [69] D. Wang *et al.*, “Clinical characteristics of 138 hospitalized patients with 2019 novel coronavirus-infected pneumonia in Wuhan, China,” *JAMA*, 2020.
- [70] H. Nishiura *et al.*, “Estimation of the asymptomatic ratio of novel coronavirus infections (COVID-19),” *medRxiv*, 2020.
- [71] E. Lavezzo *et al.*, “Suppression of COVID-19 outbreak in the municipality of Vo, Italy,” *medRxiv*, 2020.
- [72] Robert Koch-Institut (RKI), “Epidemiologisches Bulletin des Robert Koch-Instituts (Ausgabe 15/2020),” 2020. [Online]. Available: https://www.rki.de/DE/Content/Infekt/EpidBull/Archiv/2020/Ausgaben/15_20.pdf?__blob=publicationFile
- [73] L. Tindale *et al.*, “Transmission interval estimates suggest pre-symptomatic spread of COVID-19,” *medRxiv*, 2020.

Table 2: Epidemiological model parameters in units of days. Hospitalization and fatality rates α_h and α_b mentioned in the main body are estimated from COVID-19 case data in the region and is age-dependent. Log-normal parameters denote the underlying normal mean and standard deviation.

Counting process	Starts when	$\log \mathcal{N}$ parameters	Source
$M_i(t)$	$dE_i(t) = 1$	$(0.9470, 0.6669)^\ddagger$	[40]
$R_i^s(t), R_i^a(t)$	$dI_i^s(t) = 1$	$(2.6365, 0.0713)^\S$	[66–68]
$W_i(t)$	$dI_i^p(t) = 1$	$(0.7463, 0.4161)^\S$	[67]
$Y_i(t)$	$dI_i^s(t) = 1$	$(1.9358, 0.1421)^\S$	[69]
$Z_i(t)$	$dI_i^s(t) = 1$	$(2.5620, 0.0768)^\S$	[41]

Parameter	Value	Description	Source
μ	0.55	relative asymptomatic transmission rate	[33]
γ	$0.3465 h^{-1}$	decay of infectiousness at sites	[39]
δ	$4.6438 h$	non-contact contamination window [¶]	[39]
α_a	0.4	proportion of asymptomatic individuals	[38, 70, 71]

[‡] Incubation period from [40], corrected by pre-symptomatic infectiousness [67].

[§] Approximate log-normal parameters constructed because COVID-19 literature results only reported using mean or median estimates of times.

[¶] For computational purposes, set from γ by the time when rate of infection drops below 20% after leaving a site.

Table 3: Average number of visits per week per site type by individuals of different age groups.

Age group	Education	Social	Transportation	Work	Groceries
0-4	5	1	-	-	-
5-14	5	2	3	-	-
15-34	2	2	3	3	1
35-59	-	2	1	5	1
60-79	-	3	2	-	1
80+	-	2	1	-	1

A Household infections

If information about households $\mathcal{H}(i)$ that each individual $i \in \mathcal{V}$ belongs to is available, one can account for infections within households by adding the following base rate $\lambda_{\mathcal{H}(i)}(t)$ to the conditional intensity function $\lambda_i^*(t)$ of the exposure counting process $N_i(t)$:

$$\lambda_{\mathcal{H}(i)}(t) = \xi \sum_{j \in \mathcal{H}(t) \setminus i} \int_{t-\delta}^t e^{-\gamma(t-\tau)} K_{i,j}^{\mathcal{H}}(\tau) d\tau \quad (11)$$

where

$$K_{i,j}^{\mathcal{H}}(\tau) = (I_j^s(\tau) + I_j^p(\tau) + \mu I^a(\tau)) \prod_{k \in \mathcal{S}} (1 - P_{i,k}(\tau))(1 - P_{j,k}(\tau)) \quad (12)$$

where $\xi \geq 0$ is the base transmission rate within households. This intensity function models our assumption that individuals within a household are in contact as long as they are not visiting any site.

Exposure events caused by $\lambda_{\mathcal{H}(i)}(t)$ can be sampled analogously to the principles for sampling exposure times introduced in Section 3. Their superposition with exposures at sites is handled by the priority queue.

B Testing based on empirical probability of exposure

In this work, we consider the possibility of allocating tests based on the empirical exposure probability of contacts of an infectious person, as resources are often initially limited in practice [72]. We define the *empirical risk testing policy* $\pi_{\text{test}}^{\text{risk}}$ as allocating tests only to the top K individuals j of contacts $\mathcal{C}_i(t_0, t_f)$ ranked by their empirical probability of exposure $\hat{p}_{j \leftarrow i}(t_0, t_f)$ during a time window $[t_0, t_f]$ associated with i in the process $N_j(t)$:

$$\hat{p}_{j \leftarrow i}(t_0, t_f) = 1 - \exp(-K_{i,j}^C(t_0, t_f)) \quad (13)$$

with

$$K_{i,j}^C(t_0, t_f) = \sum_{k \in \mathcal{S}} \beta_k \int_{t_0}^{t_f} P_{j,k}(t') \int_{t'-\delta}^{t'} P_{i,k}(\tau) e^{-\gamma(t'-\tau)} d\tau dt' \quad (14)$$

and where the inner integral would be substituted by $P_{j,k}$ under proximity-based tracing, ignoring environmental transmission.

Disregarding second order effects and inaccuracies in estimating the empirical probability of exposure, the empirical risk testing policy can be interpreted as a greedy allocation of tests under limited resources. We leave the consideration of more sophisticated contact tracing policies for future work.

C State variable initialization

While background exposures in *Scenario B* are directly modeled by adding a constant base rate $\lambda_{0,i}^*(t)$ to $\lambda_i^*(t)$ in the exposure counting processes $N_i(t)$, *e.g.*, to model visits to neighboring regions, there need to be non-degenerate initial conditions when simulating *Scenario A* and for parameter estimation during the same period. Since COVID-19 case data is available during this time window, we opt to heuristically compute aggregate initial seed counts for the state variables. The starting point of *Scenario A* is selected such that approximately five to ten COVID-19 cases occurred.

We set the number of initially symptomatic individuals $I_{\text{init}}^s = \sum_{i \in \mathcal{V}} I_i^s(0)$ equal to the real observed COVID-19 cases in a region at the start date, or scaled proportionally to the population size in an administrative region, and set all to be positively tested. Based on the above, we seed $I_{\text{init}}^a = \alpha_a / (1 - \alpha_a) I_{\text{init}}^s$ individuals to be initially asymptomatic to obtain a proportion of recently estimated $\alpha_a = 0.4$ asymptomatic seeds [38, 70, 71]. Assuming that infectious individuals have exposed R_0 others on average, we seed $E_{\text{init}} = R_0(I_{\text{init}}^a + I_{\text{init}}^s)$ initially exposed individuals, using recent estimates of the basic reproduction number of approximately $R_0 = 2.0$ [38, 66, 73]. In a simulation of *Scenario A*, $E_i(0), I_i^a(0), I_i^s(0)$ are seeded uniformly at random following the above heuristic counts. Neither asymptomatic nor symptomatic seeds cause further exposures, and no other states are seeded for simplicity.

D Experimental setup for estimation

In this section, we provide additional details on the experimental setup used for parameter estimation, which we perform separately for each of the cities and regions. One central challenge for parameter estimation using real COVID-19 case data is that the epidemic did not evolve without interventions. The spread of COVID-19 was significantly influenced by social distancing measures and business restrictions in both Germany and Switzerland during most of the time periods for which data is available. The period of most restrictive measures, also referred to as the “lockdown”, occurred largely from March 23, 2020 to May 3, 2020 in Germany, and from March 16, 2020 to May 10, 2020 in Switzerland [51–53]. To allow for parameter estimation over the entire time period of *Scenario A*, we account for the restrictions in place during the “lockdown” by

- (i) scaling down β_k at sites of specific categories to mimic *business restrictions*. Specifically, we reduce the individual transmission rate at educational sites, workplaces and social sites by 50% during the period of the “lockdown”.

Table 4: Summary for towns and regions studied in Germany and Switzerland.

Region		$ \mathcal{V} $	$ \mathcal{S} $	Urban?	Incidence*	Lockdown
Rheingau-Taunus	GER	187,163	2,352	-	144.8	03/23
Kanton Jura	CH	73,416	729	-	355.5	03/16
Kaiserslautern	GER	104,044	1,525	✓	200.7	03/23
Bern	CH	133,790	2,174	✓	191.4	03/16
Locarno	CH	15,820	494	-	943.8	03/16
Tübingen	GER	90,539	1,446	✓	570.1	03/23

* Number of COVID-19 cases per 100,000 inhabitants before July 13, 2020, taken at *Landkreis* and *Kanton*-level from data provided by the national authorities [45, 46].

- (ii) letting individuals practice *social distancing* by skipping a given visit with probability ρ during the “lockdown”. This social distancing factor ρ is estimated, controls how strictly governmental interventions were followed in a given town, and guides how much the case curve flattened during the “lockdown”.

Note that before the “lockdown”, *i.e.*, in periods without intervention, ρ and the β_k -multipliers at sites are ignored by the model; see Table 4. Thus, we jointly estimate the exposure parameters $\theta = \{\beta, \xi, \rho\}$ over the time period that we denote as *Scenario A* for a given region, *i.e.*, for a period of approximately two months until the end of the strict “lockdown” in either country. All three parameters can be deemed identifiable because the estimation windows span periods both before and during times of interventional measures. We downsample the population and sites by a factor K uniformly at random⁸ *during estimation only* as listed in Table 5.

The estimation procedure is run for 100 steps for the computationally less demanding cities, *i.e.*, Tübingen, Kaiserslautern, and Locarno, and for a total of 40 steps for the computationally more demanding city of Bern, the Canton of Jura, and the Landkreis of Rheingau-Taunus, each including 20 initial quasi-random settings. Each evaluation of the objective for a given setting of θ is the mean of $J = 96$ random realizations of our model over the time period. Simulations are randomized across realizations of the mobility traces and the selected individual infection seeds.

The domain for β and ξ was empirically bounded to $[0, 1.5]$ in all regional models, while keeping $\rho \in [0, 1]$ as ρ is a probability. Maximization of the knowledge gradient acquisition function is done using the internal optimization procedures of BOTORCH [43].

E Parameter estimation using downscaled models might fail

While we have found that using downscaled models for parameter estimation works well in most practical scenarios, there do exist settings where it can fail. More specifically, the full-scale model may not provide accurate predictions under the parameters $\theta = \{\beta, \xi, \rho\}$ estimated using the downscaled model. In the remainder, we analyze one such setting, the Landkreis of Tirschenreuth in Germany, a rural region with a high level of infections.

With a case incidence of 1,575 cases per 100,000 inhabitants as of July 13, 2020 [45], the region is more affected than the other cities and regions we considered. During parameter estimation, 7.69% of the population in the *downscaled* model needs to get positively tested to match the COVID-19 case data in Eq. 8. In addition, sites are clustered into a number of villages, a major distinguishing factor compared to other regions with high infection levels we studied. Thus, removing a large proportion of sites at random can lead to local and isolated infection herds in which potentially large proportions of the population get infected. Considering that simulated infections might be even higher than positive test results, the proportion of susceptible people in local clusters could decrease significantly. Refer to Figure 14 for a visualization of the specific local circumstances in Tirschenreuth. To overcome the resulting reduction in infections, larger transmission rates β_k will be estimated for the model to reach the target case incidence. In contrast, under

⁸Initial state variable seeds and the COVID-19 case counts are not downscaled.

Table 5: Estimated parameters for towns and regions studied in Germany and Switzerland. β denotes the individual transmission rate at public sites, ξ the individual transmission rate in households, and ρ the social distancing factor, estimated as described in Section 4 and Appendix D using downscaling factor K .

Region		Inference period [†]	K	β	ξ	ρ
Rheingau-Taunus	GER	03/10 - 05/03	10	0.1875	0.9375	0.8750
Kanton Jura	CH	03/09 - 05/10	10	0.1406	0.7031	0.8438
Kaiserslautern	GER	03/15 - 05/03	10	0.3004	0.4548	0.6327
Bern	CH	03/06 - 05/10	10	0.4688	0.2812	0.9375
Locarno	CH	03/09 - 05/10	2	0.7607	0.5394	0.9181
Tübingen	GER	03/12 - 05/03	10	0.7450	1.0842	0.8116

[†] Chosen such that a given region had approximately five to ten confirmed COVID-19 cases, allowing for non-degenerate and comparable initial conditions. Dates are in 2020.

the full-scale model, only 1.54% of the population would have to get positively tested to match the COVID-19 case data, suggesting for the decrease in the number of susceptible individuals to have a smaller impact. As a consequence, in Landkreis Tirschenreuth, the predictions under the full-scale model are empirically found to be too pessimistic. Overall, we recommend choosing a conservative scaling factor during parameter estimation such that infection levels continue to be low enough to expect equal exposure dynamics at both scales.

F Narrowcasting the empirical probability of exposure

As recently noted by Chan et al. [63], health authorities may like to use contact tracing data of individuals who have been tested positive to *narrowcast* messages to the population, *i.e.*, make public service announcements that are highly tailored to a location or to a subset of individuals who have been in a certain location during a specific period of time. For example, health authorities may like to inform the population about the risk of infection for individuals who visited a specific site in a certain period of time. While some individuals may be reluctant to adopt contact tracing technology due to privacy concerns, they may still be willing to follow public service announcements regarding quarantine or testing. For example, an individual may be willing to self-isolate or seek testing if they learn via narrowcasting that they recently visited a location with empirically high probability of exposure by other infected individuals.

To implement narrowcasting of exposure risk at sites \mathcal{S} , our model allows for the estimation of the empirical probability of exposure $\hat{p}_k([t_0, t_f])$ of an individual during a time window $[t_0, t_f]$, caused by positively tested individuals i that visited site k , *i.e.*,

$$\hat{p}_k([t_0, t_f]) \propto 1 - \prod_{\substack{i \in \mathcal{S} \\ T_i^+(t_0)=1}} \exp \left(- \int_{t_0}^{t_f} \int_{t'-\delta}^{t'} P_{i,k}(\tau) e^{-\gamma(t'-\tau)} d\tau dt' \right) \quad (15)$$

Perhaps surprisingly, the above computation does not suffer from the “ x^2 adoption problem” of contact tracing [38, 62] because it only requires $P_{i,k}(t)$ of positively tested individuals i , rather than both $P_{i,k}(t)$ and $P_{j,k}(t)$. For the same reason, it also requires data from location-based contact tracing systems where $P_{i,k}(t)$ is observed. However, in principle, one could also resort to proximity-based tracing systems if Bluetooth beacons are in place, as noted by Langford [62].

Figure 7 presents an example of narrowcasting of site-specific exposure probabilities during *Scenario A* with the estimated “lockdown” measures. Here, note that, as long as the level of adoption is uniformly distributed across visitors, the site ranking by exposure probability will be invariant to adoption levels in expectation. In this case, the absolute value of the probability of exposure can be corrected for the level of adoption. In practice, it would be important to correct for compliance disparities across sites and site types, which are likely to occur due to differences in demographics and visiting patterns at certain sites.

Algorithm 2 Sampling algorithm for model simulation⁹

Input: Initial state variables at $t = 0$, location traces $P_{i,k}(t)$, parameters $\gamma, \delta, \alpha_a, \alpha_b, \alpha_h, \mu$ and β_k , hazard functions $\lambda_{-}(t)$

- 1: $t_{\text{now}} \leftarrow 0, S_i \leftarrow 1, Q \leftarrow$ priority queue processing in temporal order of events
- 2: **for** all $i \in \mathcal{V}$ s.t. $S_i = 0$ **do**
- 3: Push next state transition $(0, _, i, \emptyset)$ to Q (see below)
- 4: **while** Q not empty **do** $\triangleright Q$ contains (time, transition, i , infector, site) events
- 5: $(t_{\text{now}}, e, i, j, k) \leftarrow$ pop earliest from Q
- 6: **if** e is dE **and** $R_j(t_{\text{now}}) = 0$ **and** $D_j(t_{\text{now}}) = 0$ **and** $S_i = 1$ **then**
- 7: **if** $\text{INTERVENTIONS}(i, j, k, t_{\text{now}})$ **then** \triangleright Reject and re-sample?
- 8: Call Algorithm 3 with $(P, j, i, t_{\text{now}}, r = 1 - (1 - \mu)I_j^a(t_{\text{now}}))$
- 9: **else** \triangleright Person i exposed by infector j
- 10: $E_i \leftarrow 1, S_i \leftarrow 0, \Delta_M \sim \text{Expo}(\lambda_M(t_{\text{now}})), u \sim \text{Unif}(0, 1)$
- 11: **if** $u \leq \alpha_a$ **then**
- 12: Push $(t_{\text{now}} + \Delta_M, dI^a, i, \emptyset)$ event to Q
- 13: **else**
- 14: Push $(t_{\text{now}} + \Delta_M, dI^p, i, \emptyset)$ event to Q
- 15: **else if** e is dI^p **then** \triangleright Person i pre-symptomatic
- 16: $I_i^p \leftarrow 1, E_i \leftarrow 0, \Delta_Z \sim \text{Expo}(\lambda_W(t_{\text{now}}))$
- 17: Push $(t_{\text{now}} + \Delta_Z, dI^s, i, \emptyset)$ event to Q
- 18: **for** u such that $S_u = 1$ **do**
- 19: Call Algorithm 3 with arguments $(P, i, u, t_{\text{now}}, r = 1)$
- 20: **else if** e is dI^s **then** \triangleright Person i symptomatic
- 21: $I_i^s \leftarrow 1, I_i^p \leftarrow 0, u, v \sim \text{Unif}(0, 1)$
- 22: **if** $u \leq \alpha_h$ **then**
- 23: $\Delta_Y \sim \text{Expo}(\lambda_Y(t_{\text{now}})), \text{Push } (t_{\text{now}} + \Delta_Y, dH, i, \emptyset)$ event to Q
- 24: **if** $v \leq \alpha_b$ **then**
- 25: $\Delta_Z \sim \text{Expo}(\lambda_Z(t_{\text{now}})), \text{Push } (t_{\text{now}} + \Delta_Z, dD, i, \emptyset)$ event to Q
- 26: **else**
- 27: $\Delta_R \sim \text{Expo}(\lambda_{R^s}(t_{\text{now}})), \text{Push } (t_{\text{now}} + \Delta_R, dR, i, \emptyset)$ event to Q
- 28: **else if** e is dI^a **then** \triangleright Person i asymptomatic
- 29: $I_i^a \leftarrow 1, E_i \leftarrow 0, \Delta_R \sim \text{Expo}(\lambda_{R^a}(t_{\text{now}}))$
- 30: Push $(t_{\text{now}} + \Delta_R, dR, i, \emptyset)$ event to Q
- 31: **for** u such that $S_u = 1$ **do**
- 32: Call Algorithm 3 with arguments $(P, i, u, t_{\text{now}}, r = \mu)$
- 33: **else if** e is dH **then** \triangleright Person i hospitalized
- 34: $H_i \leftarrow 1$
- 35: **else if** e is dR **then** \triangleright Person i resistant
- 36: $R_i \leftarrow 1, I_i^a \leftarrow 0, I_i^s \leftarrow 0, H_i \leftarrow 0$
- 37: **else if** e is dD **then** \triangleright Person i deceased
- 38: $D_i \leftarrow 1, I_i^s \leftarrow 0, H_i \leftarrow 0$

⁹For simplicity, we omit details about the procedure $\text{INTERVENTIONS}(i, j, k, t)$, which applies thinning as explained in Section 3 due to interventional measures, and point the reader to our implementation at: <https://github.com/covid19-model/>

Algorithm 3 Pushes next event of individual i exposing individual j in time window $[t, t_{\max}]$ by considering only the contribution $\lambda_{i \rightarrow j}^*(t)$ in Eq. 6 and using thinning as described in Section 3.

Input: P, i, j, t, r ▷ Below, indicator $\mathbb{I}[\cdot]$ returns **True/False**

```

1: procedure INCONTACT( $u, v, \tau$ )
2:   return  $\mathbb{I}[\exists k \in \mathcal{S} \text{ s.t. } P_{u,k}(\tau) = 1 \text{ and } \exists \tau' \in [\tau - \delta, \tau] \text{ s.t. } P_{v,k}(\tau') = 1]$ 
3: procedure CONTACTSITE( $u, v, \tau$ )
4:   return  $k$  if  $\exists k \in \mathcal{S} \text{ s.t. } P_{u,k}(\tau) = 1 \text{ and } \exists \tau' \in [\tau - \delta, \tau] \text{ s.t. } P_{v,k}(\tau') = 1$ 
   else return  $\emptyset$ 
5: procedure NEXTCONTACT( $u, v, \tau$ )
6:   return  $\min_{\tau' > \tau} \tau' \text{ s.t. } \text{INCONTACT}(u, v, \tau')$ 
7: procedure WILLBEINCONTACT( $u, v, \tau$ )
8:   return  $\mathbb{I}[\exists \tau' \in [\tau, t_{\max}] \text{ s.t. } \text{INCONTACT}(u, v, \tau')]$ 
9:  $\tau \leftarrow t$ 
10: while WILLBEINCONTACT( $j, i, \tau$ ) do
11:    $b \leftarrow \text{INCONTACT}(j, i, \tau)$ 
12:   if not  $b$  then
13:      $\tau \leftarrow \text{NEXTCONTACT}(j, i, \tau)$ 
14:    $\Delta_{E_j} \sim \text{Expo} \left( \max_k \{\beta_k\} r \int_{\tau-\delta}^{\tau} e^{-\gamma(\tau-v)} dv \right)$ 
15:    $\tau \leftarrow \tau + \Delta_{E_j}$ 
16:   if INCONTACT( $j, i, \tau$ ) then
17:      $k \leftarrow \text{CONTACTSITE}(j, i, \tau)$ 
18:      $p \leftarrow \left( \beta_k \int_{\tau-\delta}^{\tau} e^{-\gamma(\tau-v)} P_{i,k}(v) dv \right) / \left( \max_k \{\beta_k\} \int_{\tau-\delta}^{\tau} e^{-\gamma(\tau-v)} dv \right)$ 
19:      $u \sim \text{Unif}(0, 1)$ 
20:     if  $u \leq p$  then
21:       Push  $(\tau, dE, j, i)$  event to  $Q$ 
22:       break
```

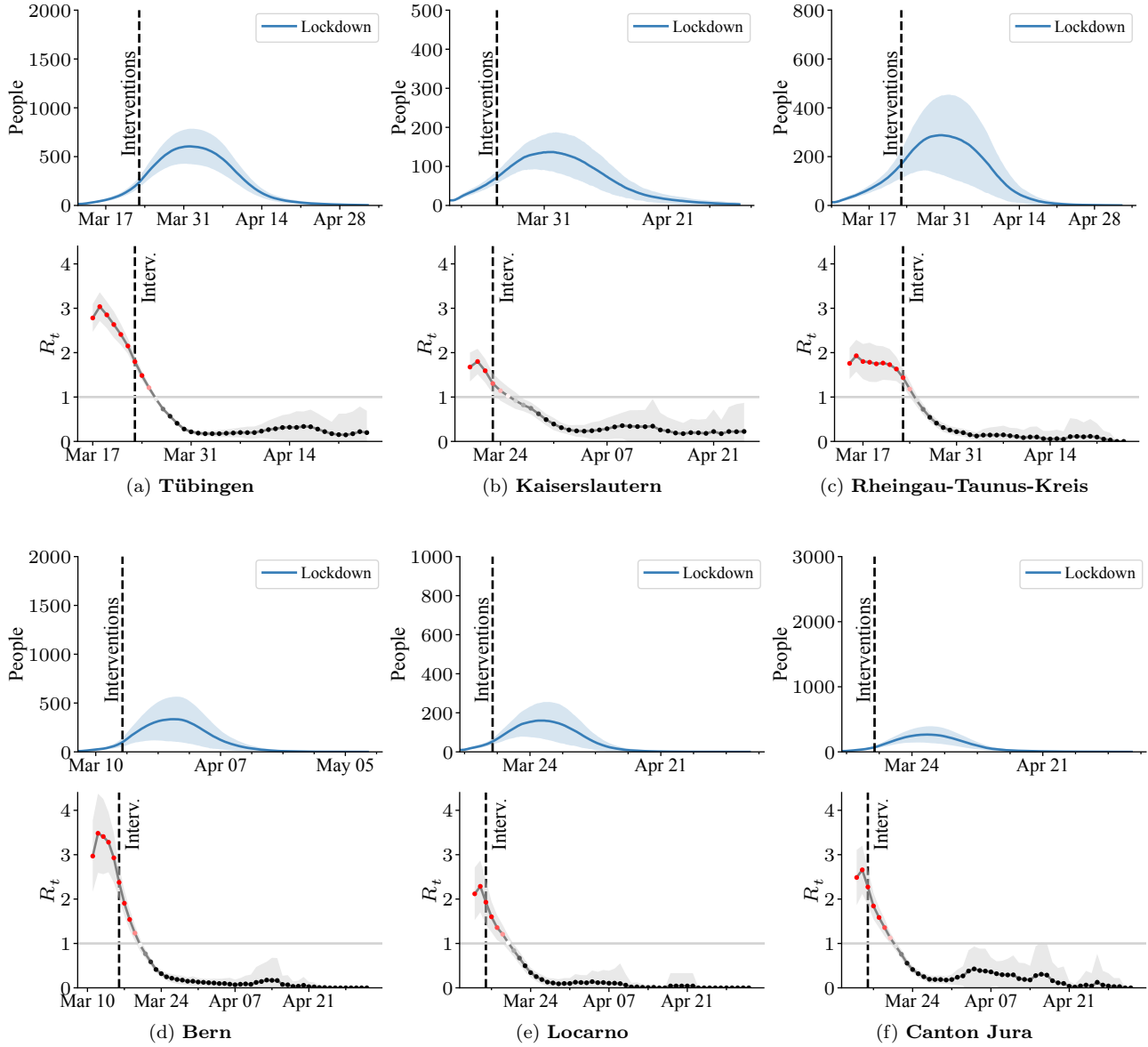


Figure 8: **Number of infected and effective reproduction number in the realistic scenario used for parameter estimation, *i.e.*, when the lockdown measures are in place as estimated.** For each region, the top panel shows the number of infected individuals, where the line represents the mean over 48 random simulations and the shaded regions indicate to two times the standard deviation. The bottom panels show the corresponding effective reproduction number computed using the approach of Athreya et al. [9], which fit a Negative-Binomial (NB) distribution to the number of secondary cases. The line represents the most likely estimate and shading represents high density areas.

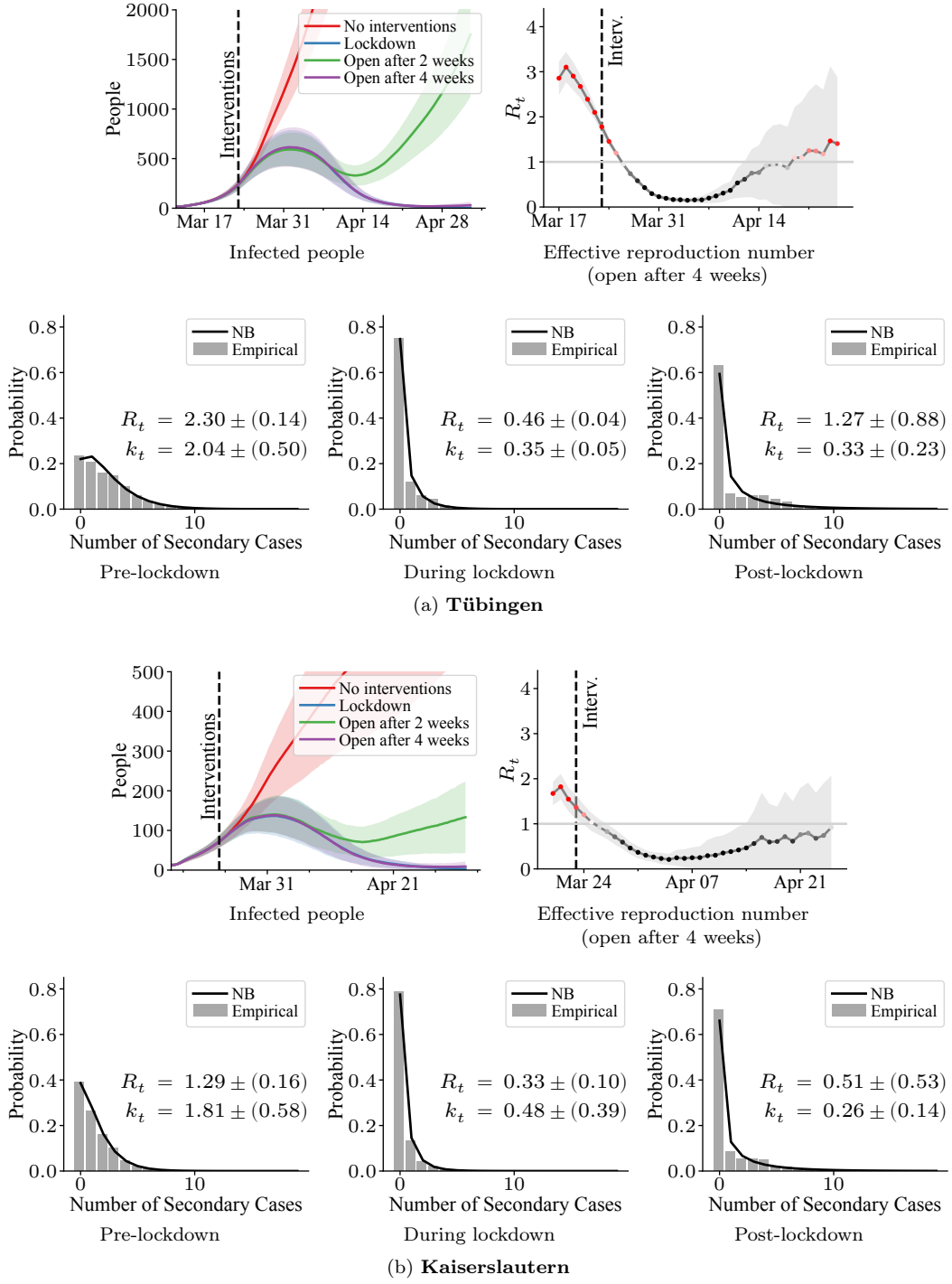


Figure 9: **Early ending “lockdown” scenario.** In each group of 5 panels for a given region, the first panel shows the number of infected individuals when the estimated lockdown measures are lifted early, with the blue “lockdown” line being equivalent to Figure 8. The lines represent the mean number of infected over 48 random simulations and the shaded regions correspond to two standard deviations. The second panels depict the effective reproduction number R_t under the approach of Athreya et al. [9], again with lines representing the most likely estimate and shadings representing high density areas. The Negative-Binomial (NB) distributions fit to the number of secondary cases are shown in the bottom three panels at different stages of the lockdown. The R_t and k_t panels are computed for the setting when measures are lifted after 4 weeks.

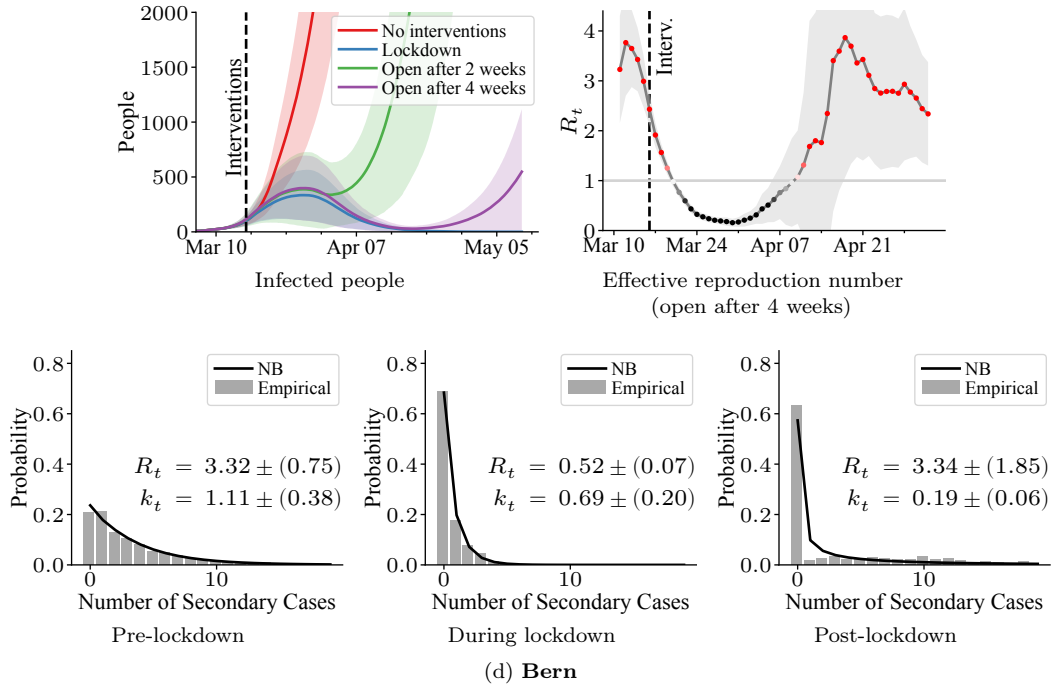
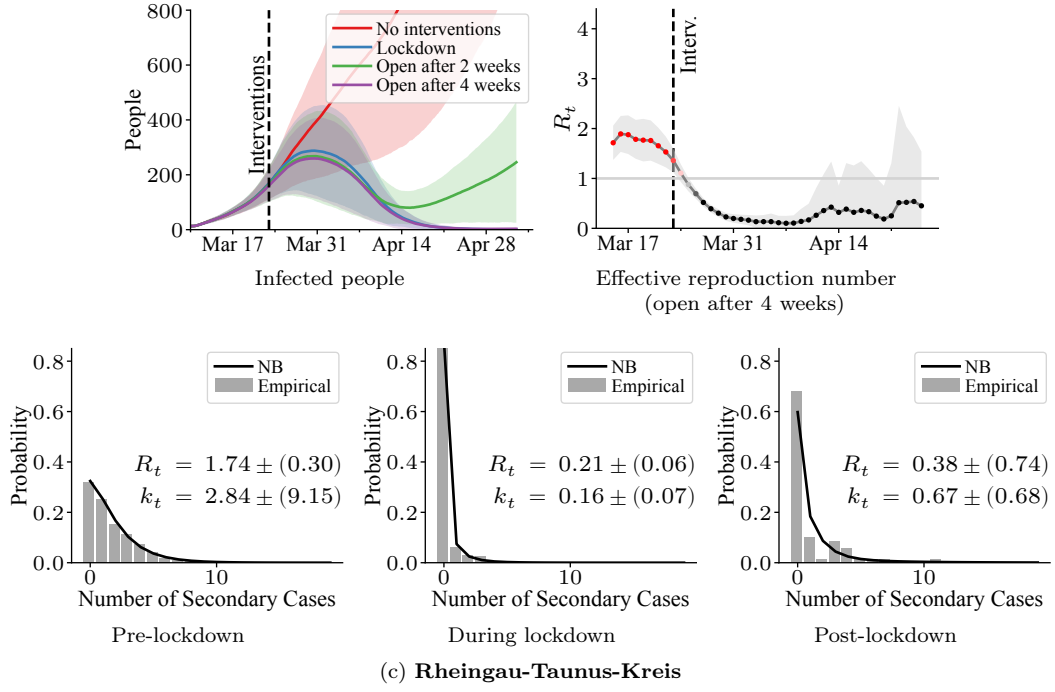


Figure 9

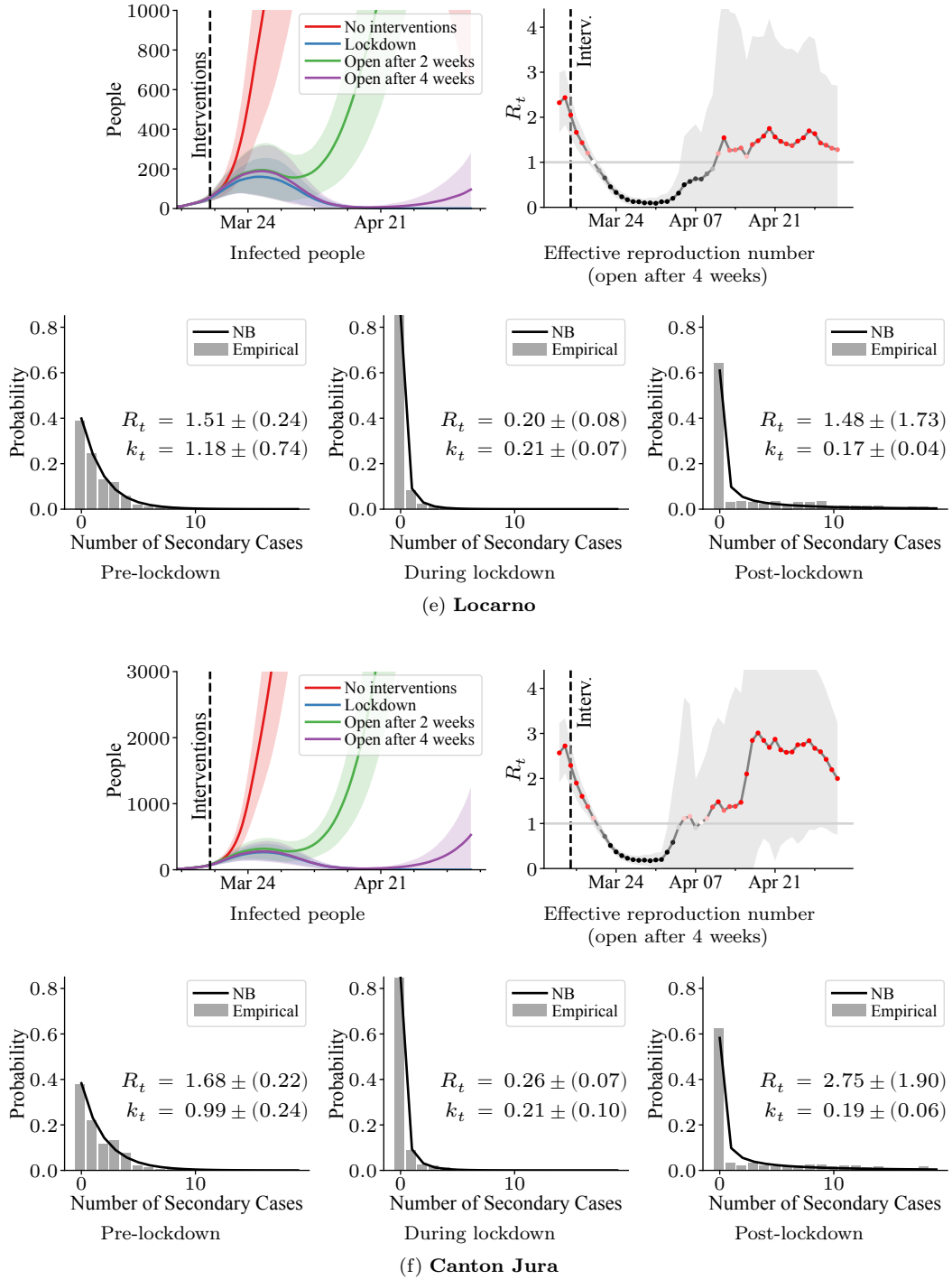


Figure 9

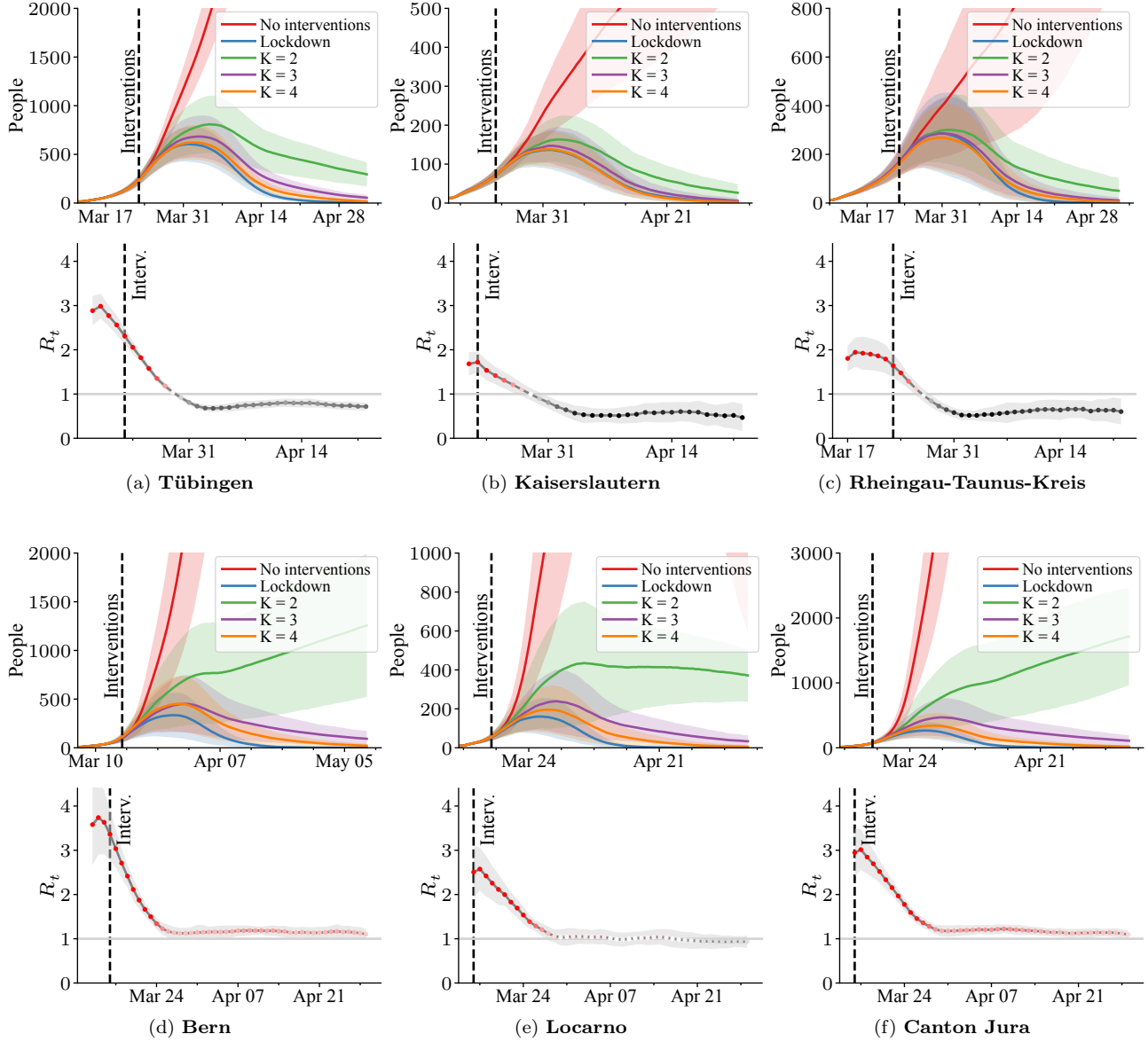


Figure 10: **Alternating curfews.** Counterfactual what-if scenario in which the population is divided into K groups and, on each day, only one group is allowed to follow their usual daily activities. For each region, the top panel shows the daily number of infected for different numbers of groups. Lines represent the mean number of infected over 48 random realizations of the model, and shaded regions correspond to two times the standard deviation. The respective bottom plots show the effective reproduction number for the scenario of $K = 2$ groups. Lines represent the most likely estimate and shadings represent high density areas, again computed using the approach of Athreya et al. [9].

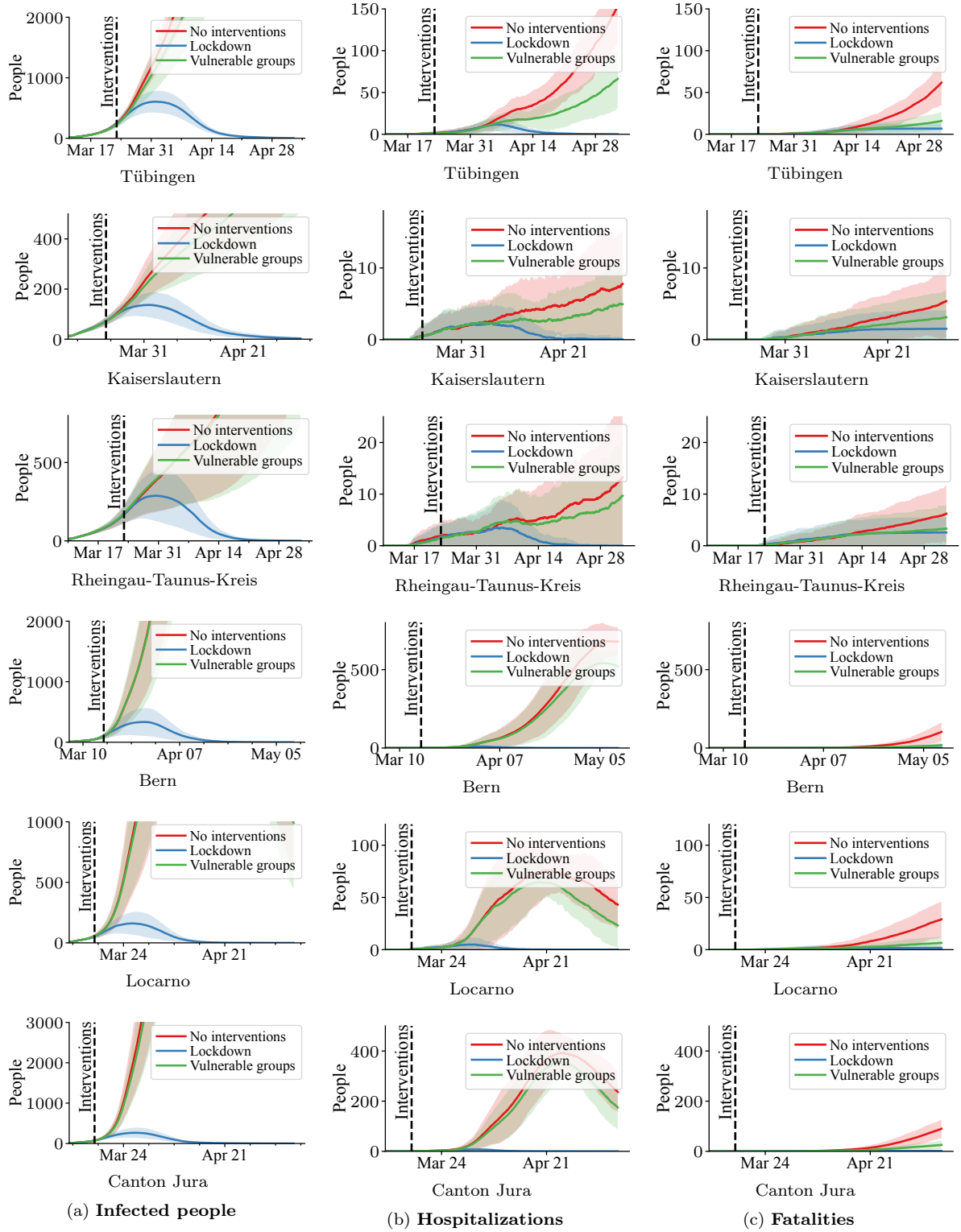


Figure 11: **Social distancing of vulnerable groups.** Counterfactual what-if scenario in which the same social distancing measures as in the “lockdown” setting are imposed on vulnerable groups only, here approximated by the group of individuals older than 60 years of age, who typically suffer more complications [45]. Panel (a) shows the daily number of infected, panel (b) and (c) the hospitalizations and fatalities, respectively. The lines represent the mean over 48 random realizations and the shaded regions correspond to two times the standard deviation.

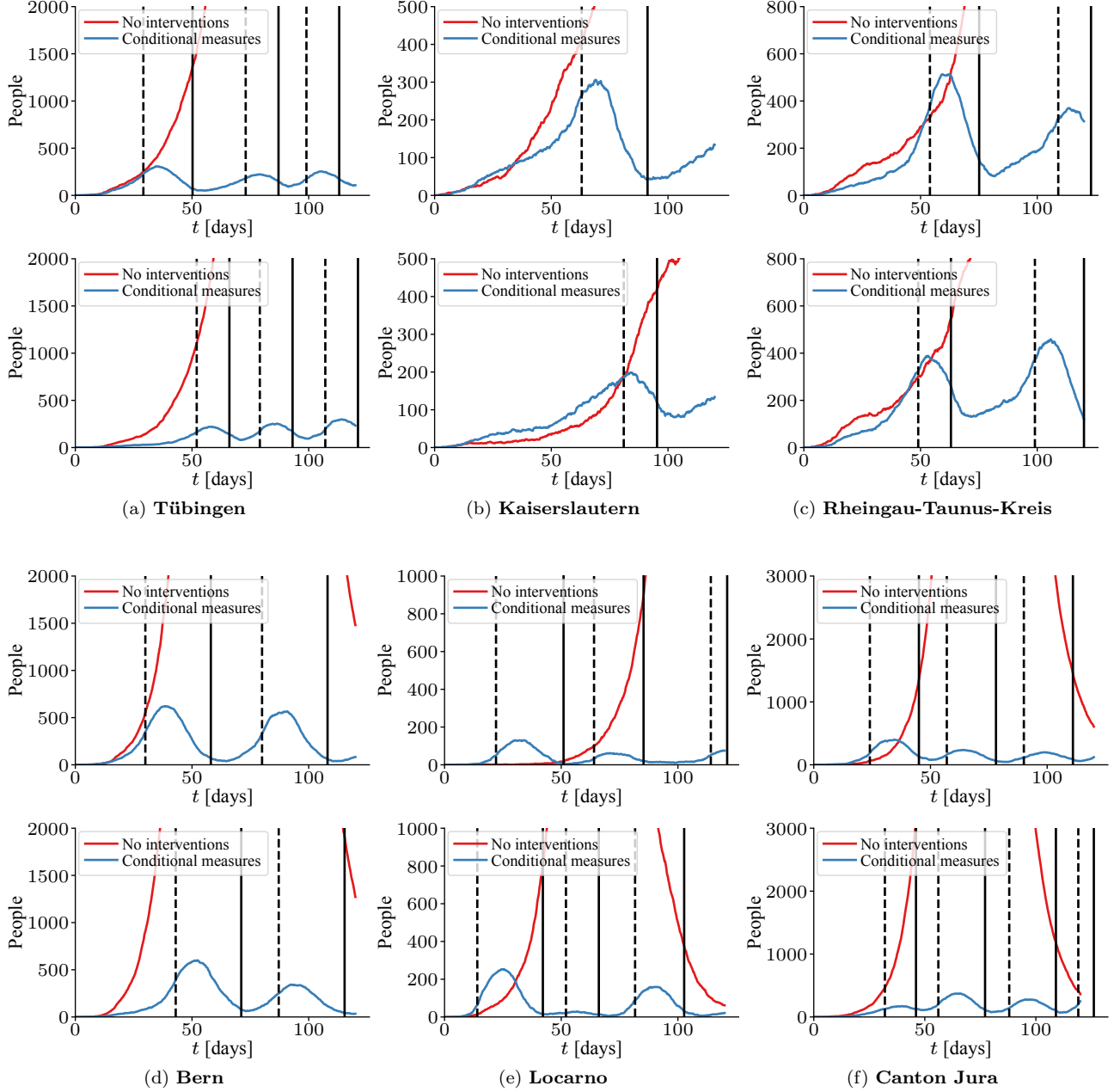


Figure 12: **Conditional “lockdowns” based on weekly incidence.** The panels show the number of infected people for two single realizations of the simulation of *Scenario B*. Whenever the number of positive cases within 7 days exceeds the threshold of 50 per 100,000 inhabitants, the same restrictive measures as in place during the “lockdown” period in *Scenario A* are implemented. Dashed and solid vertical lines indicate beginning and ending of the conditional “lockdowns”, respectively.

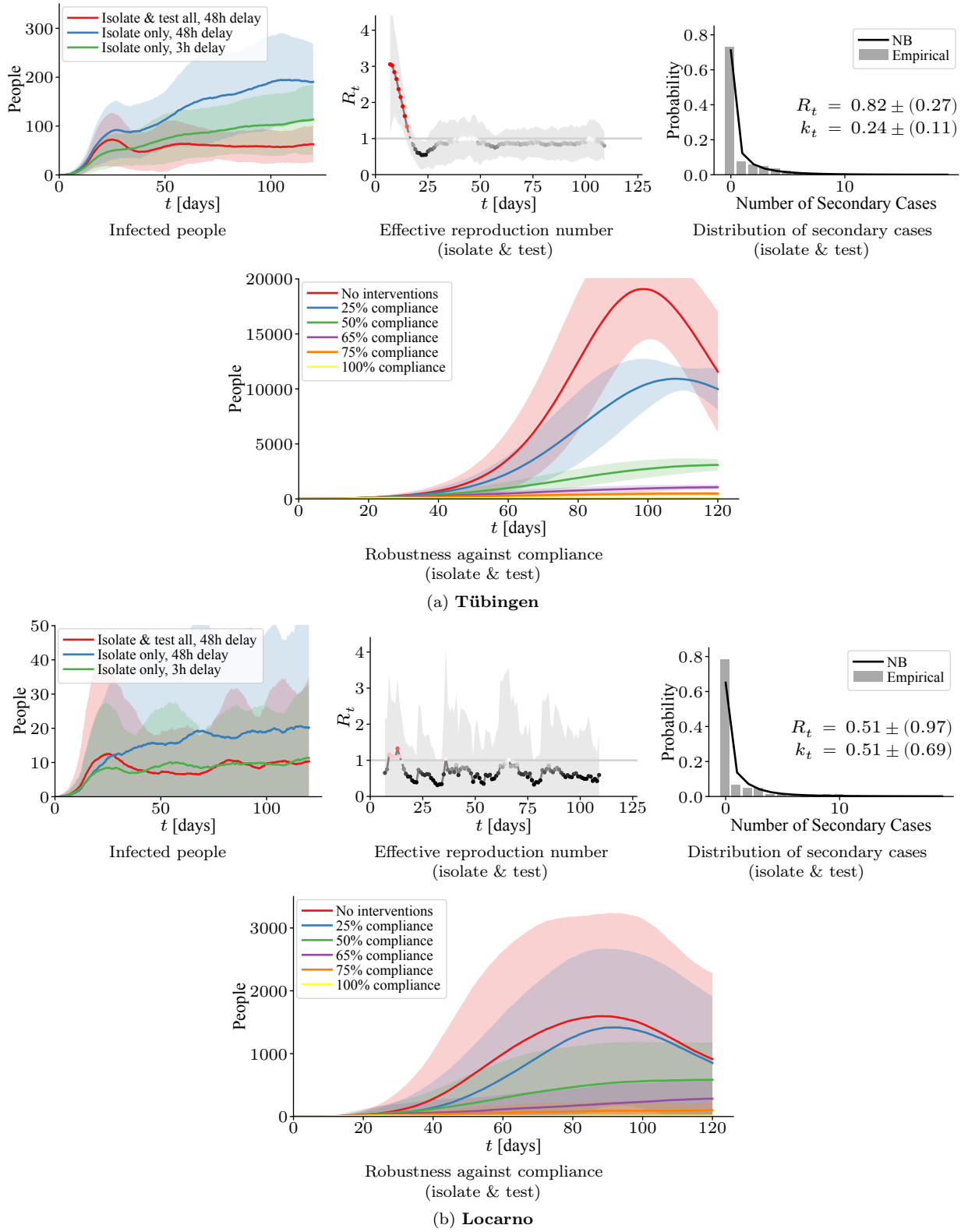
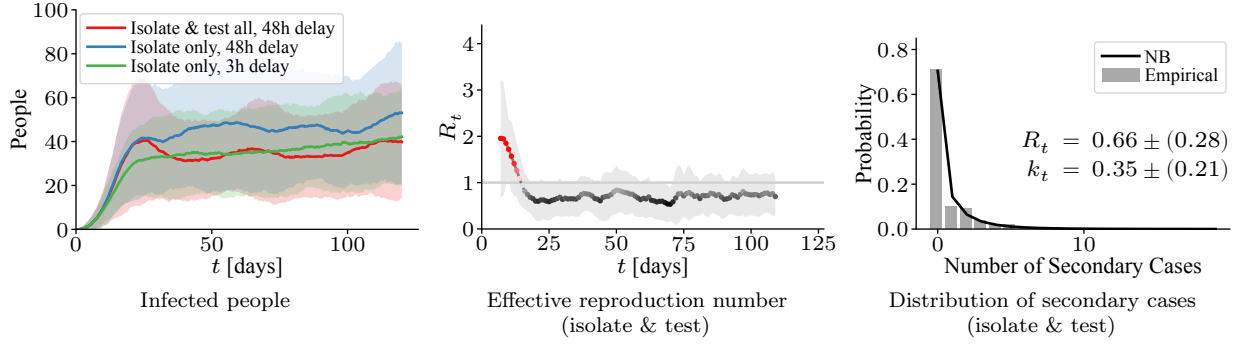
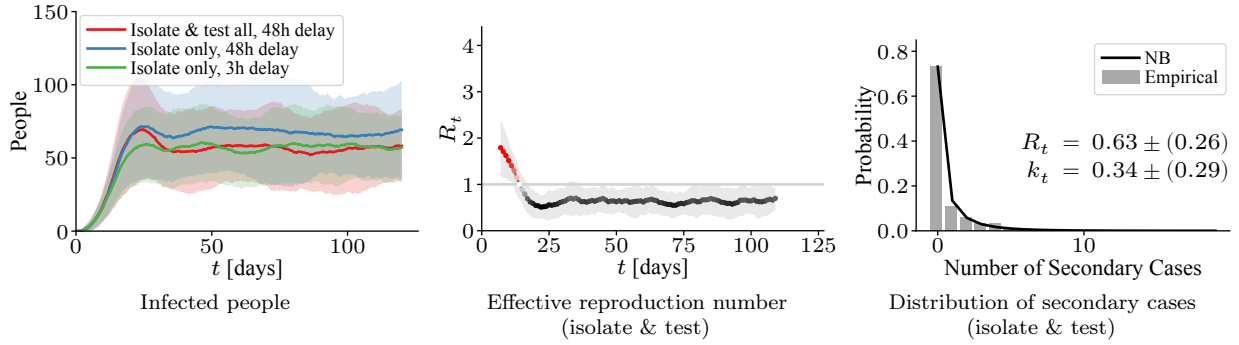


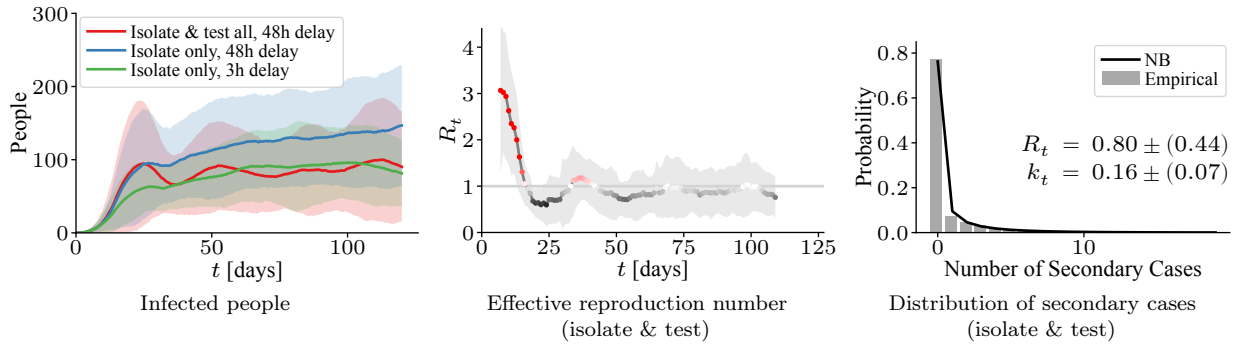
Figure 13: **Contact tracing strategies.** The three panels shown for all regions (a) - (f) show the efficacy of tracing strategies under full compliance when identified contacts are isolated and/or tested with different reporting lags. Lines and shading indicate the mean number of infected and two standard deviations over 48 random roll-outs. The effective reproduction number R_t and the distribution of secondary infections are computed as done in Figure 9. For (a) Tübingen and (b) Locarno, the larger fourth panel illustrates the efficacy of tracing when varying proportions of the population comply with the system.



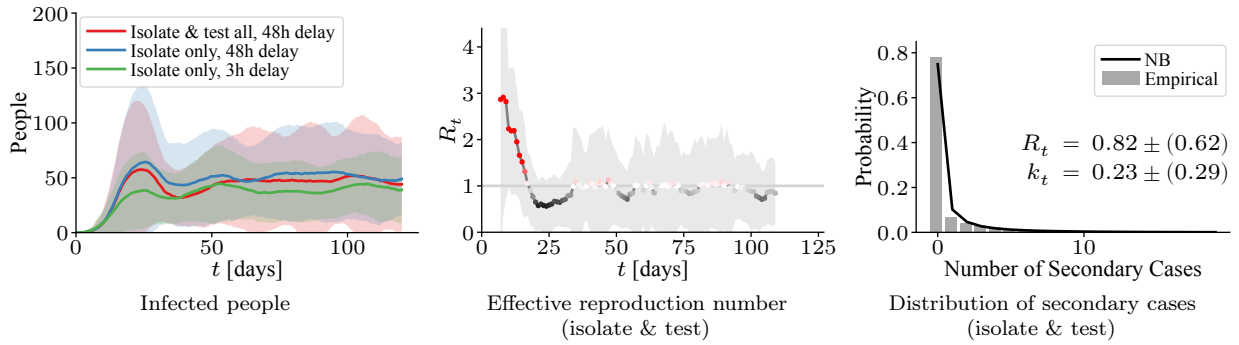
(c) **Kaiserslautern**



(d) **Rheingau-Taunus-Kreis**

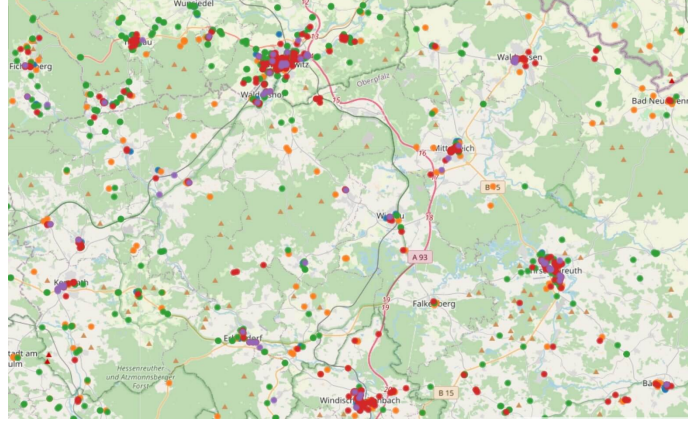


(e) **Bern**

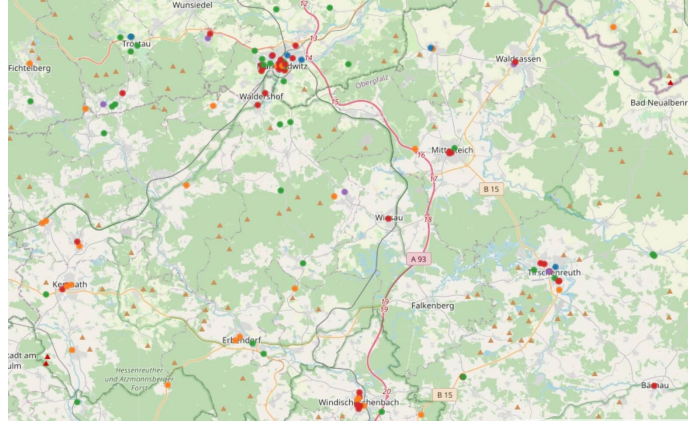


(f) **Canton Jura**

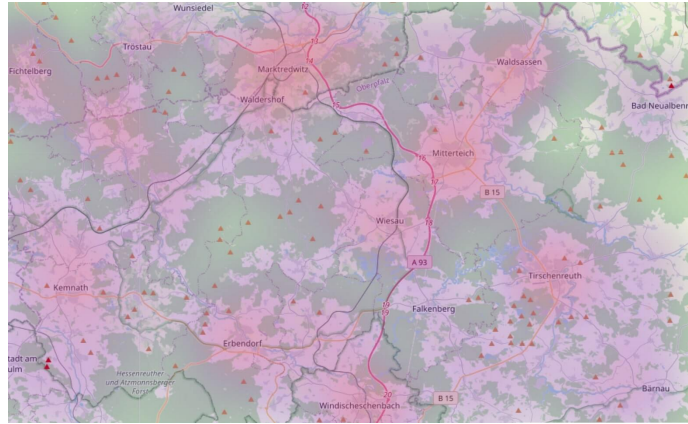
Figure 13



(a) Site locations
(full scale)

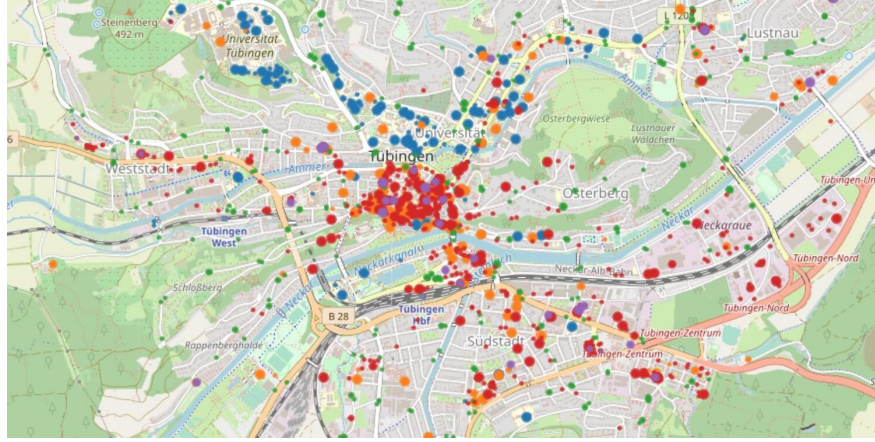


(b) Site locations
(downsampled)

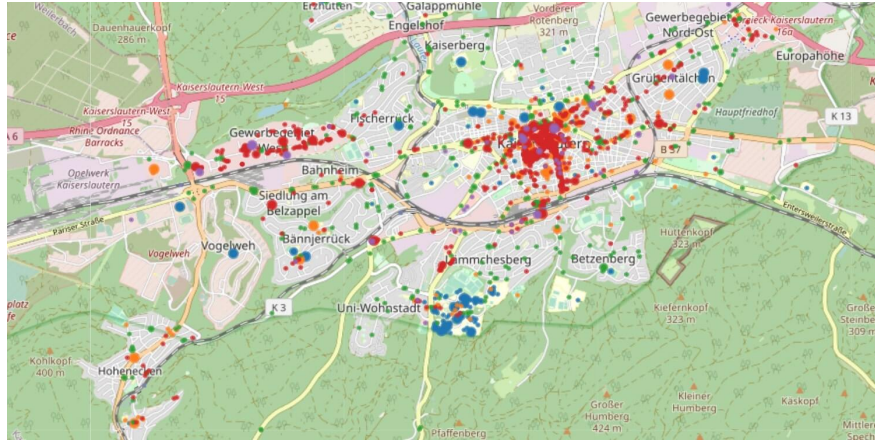


(c) Population density

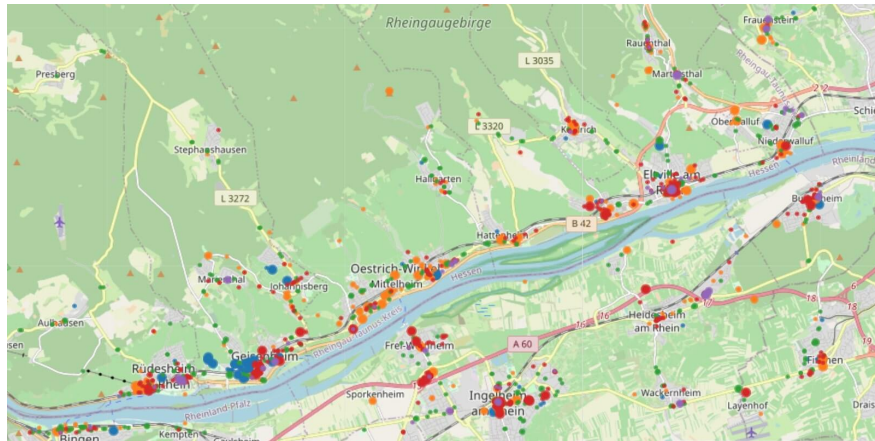
Figure 14: **Site locations and population density in Tirschenreuth, Germany.** Panel (a) shows the spatial site distribution of the full scale model of Tirschenreuth, while panel (b) depicts a downsampled model in which the number of sites is reduced by a factor of 10. Colors represent site types as defined in Figure 1. Panel (c) shows the population density taken from *Facebook Data for Good* [54]. Purple and orange colors correspond to relative low and high density of homes in the region, respectively.



(a) Tübingen

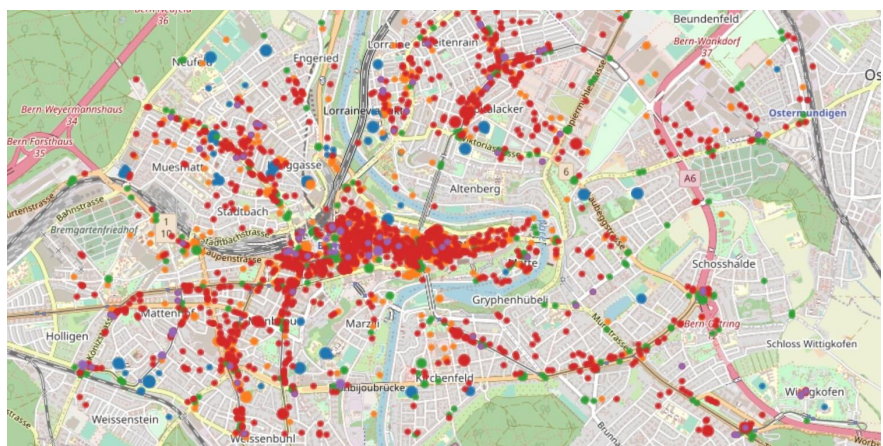


(b) Kaiserslautern

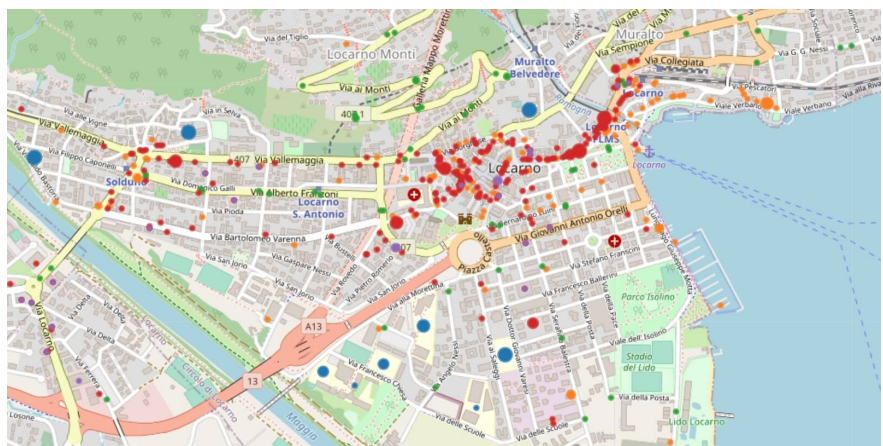


(c) Rheingau-Taunus-Kreis

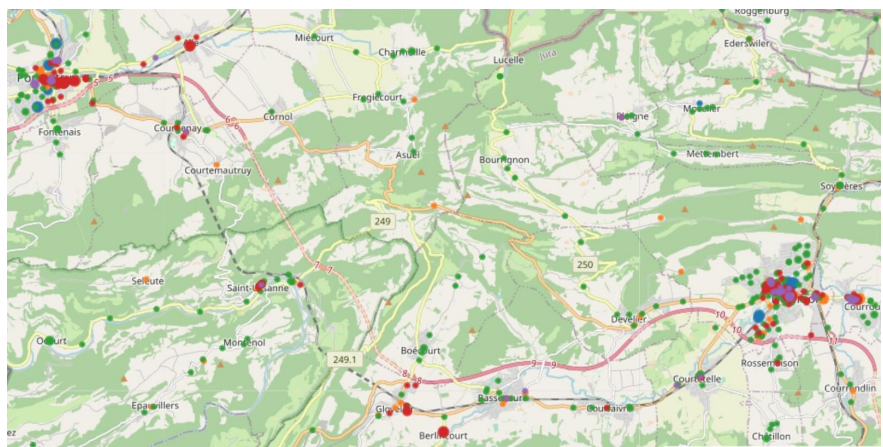
Figure 15: Narrowcasting of exposure risk at sites during a time window of two weeks of the realistic “lockdown” scenario of Figure 8. Circles represent sites and the size of each circle is proportional to the site’s empirical probability of exposure of a visiting individual during the time period. Colors represent site types as defined in Figure 1.



(d) Bern



(e) Locarno



(f) Canton Jura

Figure 15